NASA TECHNICAL REPORT

NASA TR R-447 C.1

NASA TR R-447

INVERSE SOLUTIONS FOR LAMINAR BOUNDARY-LAYER FLOWS WITH SEPARATION AND REATTACHMENT

James E. Carter
Langley Research Center
Hampton, Va. 23665

NATIONAL AERONAUTICS AND SPACE ADMINISTRATION • WASHINGTON, D. C. • NOVEMBER 1975

1. Report No.	2. Government Accession No.	3. Recipient's Catalog No.
NASA TR R-447		

4. Title and Subtitle	5. Report Date
INVERSE SOLUTIONS FOR LAMINAR BOUNDARY-LAYER FLOWS WITH SEPARATION AND REATTACHMENT	November 1975
	6. Performing Organization Code
7. Author(s)	8. Performing Organization Report No.
James E. Carter	L-10336
	10. Work Unit No.
9. Performing Organization Name and Address	505-06-31-03
NASA Langley Research Center Hampton, Va. 23665	11. Contract or Grant No.
	13. Type of Report and Period Covered
12. Sponsoring Agency Name and Address	Technical Report
National Aeronautics and Space Administration Washington, D.C. 20546	14. Sponsoring Agency Code

15. Supplementary Notes

16. Abstract

Numerical solutions of the laminar, incompressible boundary-layer equations are presented for flows involving separation and reattachment. Regular solutions are obtained with an inverse approach in which either the displacement thickness or the skin friction is specified; the pressure is deduced from the solution. A vorticity—stream-function formulation of the boundary-layer equations is used to eliminate the unknown pressure. Solutions of the resulting finite-difference equations, in which the flow direction is taken into account, are obtained by several global iteration schemes which are stable and have unconditional diagonal dominance. Results are compared with Klineberg and Steger's separated boundary-layer calculations, and with Briley's solution of the Navier-Stokes equations for a separated region. In addition, an approximate technique is presented in which the streamwise convection of vorticity is set equal to zero in the reversed flow region; such a technique results in a quick forward-marching procedure for separated flows.

17. Key Words (Suggested by Author(s))	18. Distribution Statement
Boundary-layer separation Finite-difference technique Incompressible flow	Unclassified – Unlimited Subject Category 02

19. Security Classif. (of this report)	20. Security Classif. (of this page)	21. No. of Pages	22. Price*
Unclassified	Unclassified	63	$4.25

*For sale by the National Technical Information Service, Springfield, Virginia 22161

CONTENTS

Page

INVERSE SOLUTIONS FOR LAMINAR BOUNDARY-LAYER FLOWS WITH SEPARATION AND REATTACHMENT

James E. Carter
Langley Research Center

SUMMARY

Numerical solutions of the laminar, incompressible boundary-layer equations are presented for flows involving separation and reattachment. Regular solutions are obtained with an inverse approach in which either the displacement thickness or the skin friction is specified; the pressure is deduced from the solution. A vorticity—stream-function formulation of the boundary-layer equations is used to eliminate the unknown pressure. Solutions of the resulting finite-difference equations, in which the flow direction is taken into account, are obtained by several global iteration schemes which are stable and have unconditional diagonal dominance. Results are compared with Klineberg and Steger's separated boundary-layer calculations, and with Briley's solution of the Navier-Stokes equations for a separated region. In addition, an approximate technique is presented in which the streamwise convection of vorticity is set equal to zero in the reversed flow region; such a technique results in a quick forward-marching procedure for separated flows.

INTRODUCTION

Despite the recent advances made in computer technology and computational techniques, numerical solutions of the Navier-Stokes equations for separated flows are still impractical for many applications and in many instances are unnecessary. There is growing evidence that the boundary-layer equations provide a reasonably accurate model for separated flows of limited extent. For example, good agreement with experiment was obtained by Klineberg and Lees (ref. 1) by using an integral technique to solve the boundary-layer equations for a supersonic, separated flow over a compression corner. More recently, similar calculations were made by Dwoyer (ref. 2) and by Werle and Vatsa (ref. 3) using finite-difference techniques which were in good agreement with experimental results as well as with the Navier-Stokes computations made by Carter (ref. 4). Similarly, Ghia and Davis (ref. 5) concluded from their numerical solutions of the incompressible Navier-Stokes equations for separated flows that the boundary-layer equations appear to be adequate for flows with small separation regions provided that displacement

effects are appropriately considered. These results warrant the further examination of the applicability of the boundary-layer equations for describing separated flows. In the present report some additional understanding of their applicability is provided through the examination of results obtained by two solution techniques for the laminar boundary-layer equations for incompressible flow.

As pointed out by Brown and Stewartson (ref. 6), it is generally agreed that the solution of the boundary-layer equations with a prescribed pressure gradient results in a singularity at the separation point. Many numerical investigations such as those made by Terrill (ref. 7), by Werle and Davis (ref. 8), and by Klineberg and Steger (ref. 9) support this conclusion. In all of these investigations, good agreement was obtained with Goldstein's (ref. 10) analytical results near separation. In supersonic flow the singularity at separation can be eliminated by modifying the pressure distribution through viscous-inviscid interaction. At each streamwise station the pressure calculation is coupled to the growth of the boundary layer through the use of the Prandtl-Meyer or tangent-wedge relationship. In subsonic flow the inviscid flow is elliptic. Therefore, such a procedure is not possible because the surface-pressure distribution is dependent on the entire body shape; the entire boundary-layer flow has to be taken into account before its effect on the inviscid flow can be calculated.

Several numerical investigations have demonstrated that regular solutions of the boundary-layer equations at separation can be obtained (excluding interaction) by specifying either the displacement thickness or the wall-shear stress distribution; the pressure distribution is deduced from the resulting solution. Catherall and Mangler (ref. 11) were the first to demonstrate that the boundary-layer equations could be numerically integrated past the separation point (without a singularity) by prescribing the displacement thickness distribution. With the wall shear prescribed, Kuhn and Nielsen (ref. 12) presented calculations in which they used an integral technique to solve the turbulent boundary-layer equations for separated flow. Klineberg and Steger (ref. 9) and, more recently, Horton (ref. 13) used finite-difference techniques to solve the laminar boundary-layer equations with the wall shear prescribed. In all of these calculations the singularity usually present at separation was eliminated. Another inverse procedure, which was developed earlier by Klineberg and Steger (ref. 14) and later used by Tai (ref. 15), is to use the transverse velocity at the boundary-layer edge as the prescribed condition. Since the edge value of the normal velocity component is related to the streamwise growth of the displacement thickness, this procedure is somewhat analogous to specifying the displacement thickness.

Inverse procedures have been used for attached flow as well as for separated flow. For example, Keller and Cebeci (ref. 16) developed an inverse calculation procedure for calculating attached laminar flow for a specified wall shear. Cebeci and Witherspoon

(ref. 17) modified the procedure to study incipient turbulent separation including the effects of suction at the wall.

In contrast with these inverse techniques, Briley and McDonald (ref. 18) have made calculations for subsonic flow using a direct procedure. In this procedure the unsteady boundary-layer equations are repeatedly solved until a steady-state solution is obtained. After each time step, the prescribed pressure is updated from thin airfoil theory, thereby accounting for the displacement thickness interaction. Although this technique seems feasible, it needs further examination since Briley and McDonald obtained a regular solution at a laminar separation point for a case with no interaction. This result is probably because of their use of a first-order scheme in the streamwise convection terms. As shown by Werle and Davis (ref. 8) and Klineberg and Steger (ref. 9), such a scheme requires a very fine mesh in order to resolve the separation singularity. Hence, in those cases in which interaction was included, it is not clear whether the solution at separation would be regular if a second-order scheme were used.

In the present report, which is based in part on references 19 and 20, numerical solutions of the incompressible, laminar boundary-layer equations for flows with separation and reattachment are presented. Solution techniques for either a prescribed displacement thickness or wall shear are described. In a complete calculation of a viscous-inviscid interaction, this boundary-layer computation would be matched to a calculation of the inviscid flow and this process then iterated until convergence. In the present report no viscous-inviscid interaction is considered; however, in a recent paper by Carter and Wornom (ref. 21), the prescribed displacement thickness method was combined with an inverse inviscid-flow analysis to compute a subsonic viscous-inviscid flow interaction. In addition to the interaction considerations, prescribing the displacement thickness provides a useful scaling function for the normal coordinate y, thereby eliminating boundary-layer growth in the computational coordinate $\eta = y/\delta^*$, where δ^* is the displacement thickness and η is the transformed normal coordinate. Therefore, this approach has received the main emphasis in the present study, although some calculations, mainly for comparative purposes, have been made with the wall shear prescribed. With the wall shear prescribed, several calculations were found to give discontinuous solutions. In an effort to explain these discontinuities, three different formulations of the boundary-layer equations for a prescribed wall shear are considered.

Catherall and Mangler (ref. 11), in their numerical study of separated flow, did not account for the reversed flow direction in their finite-difference scheme. In reference 11, the same finite-difference scheme was used in the reversed flow region as the scheme used for attached flow; hence, only one streamwise pass was made through the boundary layer. Since integration of the boundary-layer equations may be unstable in a direction opposite to that of the flow, it is not surprising that Catherall and Mangler encountered problems in convergence of the column iteration in the reversed flow region. In the

present report the lack of convergence found by Catherall and Mangler in the reversed flow region is overcome either by the use of a global iterative procedure or by an approximate forward-marching technique. In the global scheme, the finite-difference approximation for the streamwise convection term is switched from a backward to a forward difference in the reversed flow region to account properly for the flow direction. Klineberg and Steger (ref. 9) used a similar procedure in their numerical computation of separated flow. With the global scheme, the solution region must extend to a point downstream of reattachment to avoid the requirement of specifying the unknown downstream boundary conditions in the reverse flow region. This scheme requires repeated sweeps from the upstream boundary through reattachment until convergence is obtained.

An approximate forward-marching scheme is presented for a prescribed displacement thickness in which the streamwise convection of vorticity is neglected in the reverse flow region. The resulting procedure for obtaining approximate solutions for separated flows is quite rapid and requires only modest computer storage since the procedure is essentially the same as the usual forward-marching technique used to solve attached flows. This approximation is similar to that used by Reyhner and Flügge-Lotz (ref. 22); they were the first to show that a stable calculation can be obtained in marching through a reversed flow region if the streamwise convection of momentum is set equal to zero. Werle, Polak, and Bertke (ref. 23) and Williams (ref. 24) have also used this approximation in their calculations.

This report is divided into a number of major headings and subsections to aid the reader. In the first two major headings after the symbols list, the prescribed displacement thickness and the prescribed wall-shear methods are discussed, respectively. In these sections both the mathematical formulations as well as the numerical procedures are presented. The stability of the various finite-difference schemes used in these inverse methods is examined with the von Neumann analysis; this analysis is presented in appendixes A and B. The results obtained with these two inverse procedures are then presented separately in the "Results and Discussion" section.

SYMBOLS

A_n, B_n, C_n, D_n	coefficients in tridiagonal system of equations
C_f	skin-friction coefficient
C_n', D_n'	coefficients in Thomas algorithm
C_Z	coefficient defined in equation (81)

C_η	coefficient defined in equation (20)
C_ξ	coefficient defined in equation (19)
E_n, K_n, L_n	coefficients in recurrence equation for stream function
f	scaling function for normal coordinate
g	amplification factor
j	global iteration counter
L	reference length
M_∞	free-stream Mach number
$\hat{m}$	pressure-gradient parameter
m,n	indices for ξ- and η-directions, respectively
q	column iteration counter
R_∞, L	free-stream Reynolds number, $\frac{\rho_\infty U_\infty L}{\mu_\infty}$
r	relaxation factor
S	stream function obtained from column solution
t	time
Δt	time increment
U_∞	free-stream velocity
u	velocity component parallel to surface divided by U_∞
$\hat{u}$	$= \frac{u}{u_e}$
u_b	boundary velocity divided by U_∞

u_e	velocity component parallel to surface at boundary-layer edge divided by U_∞
v	velocity component normal to surface divided by U_∞
$\bar{v}$	$= v\sqrt{R_{\infty,L}}$
$\hat{v}$	transformed normal velocity component
W	vorticity obtained from tridiagonal equations
x	coordinate along surface divided by L
y	coordinate normal to surface divided by L
$\bar{y}$	$= y\sqrt{R_{\infty,L}}$
$\hat{y}$	transformed normal coordinate
α	coefficient of artificial time term
$\hat{\alpha}$	parameter in prescribed wall shear
δ^*	displacement thickness divided by L
$\bar{\delta}^*$	$= \delta^*\sqrt{R_{\infty,L}}$
η	transformed normal coordinate
$\Delta\eta$	grid spacing in η-direction
θ	ξ argument in von Neumann analysis
λ	Meksyn pressure-gradient parameter
μ_∞	molecular viscosity coefficient
ξ	transformed x-coordinate
$\Delta\xi$	grid spacing in ξ-direction

ρ_∞ free-stream density

$\hat{\tau}$ transformed shear

$\hat{\tau}_o$ transformed wall shear

ϕ η argument in von Neumann analysis

ψ stream function divided by $U_\infty L$

$\overline{\psi}$ $= \psi\sqrt{R_{\infty,L}}$

$\tilde{\psi}$ transformed stream function in prescribed displacement thickness method

$\hat{\psi}$ transformed stream function in prescribed wall-shear method

ω vorticity divided by U_∞/L

$\overline{\omega}$ $= \omega\Big/\sqrt{R_{\infty,L}}$

ω_o prescribed wall vorticity divided by U_∞/L

PRESCRIBED DISPLACEMENT THICKNESS METHOD

Governing Equations and Boundary Conditions

The nondimensional boundary-layer equations for two-dimensional, laminar, incompressible flow can be written as

$$\frac{\partial u}{\partial x} + \frac{\partial \bar{v}}{\partial \bar{y}} = 0 \tag{1}$$

$$u\frac{\partial u}{\partial x} + \bar{v}\frac{\partial u}{\partial \bar{y}} = u_e\frac{du_e}{dx} + \frac{\partial^2 u}{\partial \bar{y}^2} \tag{2}$$

with the boundary conditions

$$u(x,0) = \bar{v}(x,0) = 0 \tag{3}$$

and

$$u(x,y) \to u_e(x) \quad \text{as} \quad \bar{y} \to \infty \tag{4}$$

where u_e is the velocity at the edge of the boundary layer. All barred quantities have been scaled in the usual manner by the Reynolds number and are given in detail in the list of symbols. The detailed derivation and discussion of these equations and boundary conditions are presented by Schlichting (ref. 25).

This formulation is modified for the present application by first eliminating the unknown edge velocity u_e from the problem. Taking the $\bar{y}$-derivative equation (2) and introducing the vorticity $\overline{\omega} = \partial u/\partial \bar{y}$ results in

$$u \frac{\partial \overline{\omega}}{\partial x} + \bar{v} \frac{\partial \overline{\omega}}{\partial \bar{y}} = \frac{\partial^2 \overline{\omega}}{\partial \bar{y}^2} \tag{5}$$

In order to eliminate the edge velocity from the outer boundary condition, it is convenient to introduce the stream function

$$\left.\begin{aligned} u &= \frac{\partial \overline{\psi}}{\partial \bar{y}} \\ \bar{v} &= -\frac{\partial \overline{\psi}}{\partial x} \end{aligned}\right\} \tag{6}$$

The first part of equation (6) can be combined with the displacement thickness

$$\bar{\delta}^* = \int_0^\infty \left(1 - \frac{u}{u_e}\right) d\bar{y} \tag{7}$$

to show that as $\bar{y} \to \infty$

$$\overline{\psi} \to u_e(\bar{y} - \bar{\delta}^*) \tag{8}$$

Therefore, if a transformed stream function is introduced

$$\tilde{\psi} = \overline{\psi} - u(\bar{y} - \bar{\delta}^*) \tag{9}$$

then equation (4) may be replaced by

$$\tilde{\psi} \to 0 \quad \text{as} \quad \bar{y} \to \infty \tag{10}$$

If the independent variables are transformed by

$$\left.\begin{aligned} \xi &= x \\ \eta &= \frac{\bar{y}}{\bar{\delta}^*} \end{aligned}\right\} \tag{11}$$

and if equations (6) and (9) are combined and substituted into equations (1) and (2), then the governing equations become

$$u\bar{\delta}^{*2}\frac{\partial\overline{\omega}}{\partial\xi} - \bar{\delta}^*\left\{\frac{\partial}{\partial\xi}\left[\tilde{\psi} + (\eta - 1)(u\bar{\delta}^*)\right]\right\}\frac{\partial\overline{\omega}}{\partial\eta} = \frac{\partial^2\overline{\omega}}{\partial\eta^2} \tag{12}$$

$$\frac{\partial\tilde{\psi}}{\partial\eta} = \bar{\delta}^{*2}(1 - \eta)\overline{\omega} \tag{13}$$

subject to the boundary conditions

$$u(\xi,0) = \tilde{\psi}(\xi,0) = 0 \tag{14}$$

$$\left.\begin{aligned} \overline{\omega}(\xi,\eta) &\to 0 \\ \tilde{\psi}(\xi,\eta) &\to 0 \end{aligned}\right\} \quad \text{as} \quad \eta \to \infty \tag{15}$$

The transformed stream function given in equation (9) does not eliminate the u component of velocity from the governing equations. However, once the vorticity is deduced from equation (12), then u is given by

$$u(\xi,\eta) = \bar{\delta}^* \int_0^\eta \overline{\omega}(\xi,\eta_1)\, d\eta_1 \tag{16}$$

where $u(\xi,0) = 0$ has been used. For a given displacement thickness distribution, the use of equations (12), (13), and (16) subject to the boundary conditions of equations (14) and (15) results in a description of the boundary-layer flow in which the explicit appearance of the unknown edge velocity u_e has been eliminated. Unless otherwise noted, in the remainder of this paper the bars, which have been previously used to denote Reynolds number scaling, are deleted.

Numerical Technique: Global Iteration

Finite-difference scheme.- The governing equations are replaced by finite-difference expressions which depend on whether the flow is forward ($u \geqq 0$) or reversed ($u < 0$). The presence of the reverse flow region requires repeated sweeps from the upstream boundary, which is located upstream of the separation point, to a point downstream of reattachment. This sweep procedure is termed a global iteration scheme and is described in this section. Figure 1 gives a schematic diagram which shows the computational molecules used in the forward and reversed flow regions for the vorticity equation both for the prescribed displacement thickness approach and for one of several wall-shear prescribed approaches. The figure also specifies the boundary conditions. The indices m and n denote $\xi = m\,\Delta\xi$ and $\eta = n\,\Delta\eta$ and the cross in the center of the computational molecule denotes the point at which equation (12) is evaluated. In the forward flow regions it was found to be imperative to maintain second-order accuracy, and thus equation (12) is evaluated with the Crank-Nicholson scheme at the point $\xi = \left(m - \frac{1}{2}\right)\Delta\xi$, $\eta = n\,\Delta\eta$.

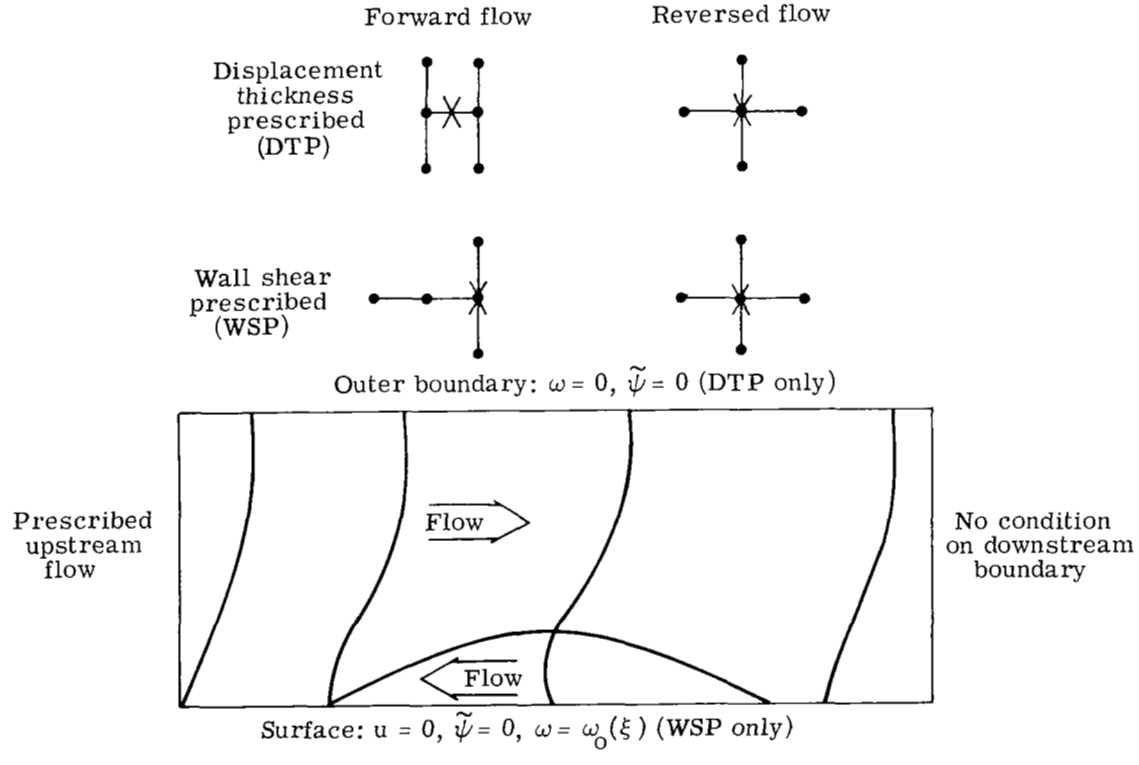

Figure 1.- Computational schemes and boundary conditions used for boundary-layer equations.

In the reversed flow regions first-order accuracy in the ξ derivative was found to be adequate; hence, a first-order forward-difference expression is substituted for $\partial\omega/\partial\xi$. Instabilities were encountered when the same forward-difference approximation was used on $\partial\tilde{\psi}/\partial\xi$ and on $\partial u\delta^*/\partial\xi$. These instabilities are eliminated when central-difference expressions are used for these terms. In the reversed flow region, $\partial\omega/\partial\eta$ and $\partial^2\omega/\partial\eta^2$ are approximated by central-difference expressions; the same approximation is used in the forward flow region.

In both the forward and reversed flow regions the finite-difference representation of equation (12) can be written as

$$A_n\omega_{m,n-1} + B_n\omega_{m,n} + C_n\omega_{m,n+1} = D_n \tag{17}$$

If the flow is forward

$$\left.\begin{aligned} A_n &= -\frac{1}{2}\left(C_\eta + 1\right) \\ B_n &= 1 + 2C_\xi \\ C_n &= \frac{1}{2}\left(C_\eta - 1\right) \\ D_n &= -A_n\omega_{m-1,n-1} + \left(2C_\xi - 1\right)\omega_{m-1,n} - C_n\omega_{m-1,n+1} \end{aligned}\right\} \tag{18}$$

where

$$C_\xi = \frac{\Delta\eta^2}{2\,\Delta\xi}\left(u\delta^{*2}\right)\Big|_{m-\frac{1}{2},n} \tag{19}$$

$$C_\eta = -\frac{\Delta\eta}{2}\left\{\delta^*\,\frac{\partial}{\partial\xi}\left[\tilde{\psi} + (\eta - 1)(u\delta^*)\right]\right\}\Bigg|_{m-\frac{1}{2},n} \tag{20}$$

In equations (19) and (20) average values are used for the required quantities at $\xi = \left(m - \frac{1}{2}\right)\Delta\xi$. In equation (20) a central difference is used for the ξ derivative. If the flow is reversed, then

$$\left.\begin{aligned} A_n &= -\left(C_\eta + 1\right) \\ B_n &= 2\left(1 - C_\xi\right) \\ C_n &= C_\eta - 1 \\ D_n &= -2C_\xi \omega_{m+1,n} \end{aligned}\right\} \tag{21}$$

where

$$C_\xi = \frac{\Delta\eta^2}{2\,\Delta\xi}\left(u\delta^{*2}\right)_{m,n} \tag{22}$$

$$C_\eta = -\frac{\delta^*_m\,\Delta\eta}{2}\frac{\partial}{\partial\xi}\left[\tilde{\psi} + (\eta - 1)(u\delta^*)\right]\Bigg|_{m,n} \tag{23}$$

No blending between the forward and reversed flow difference expressions such as that used by Klineberg and Steger (ref. 9) was used in the present iterative calculations.

Repeated application of equation (17) from the wall to the outer boundary results in a tridiagonal system of linear equations for the vorticity if the coefficients A_n, B_n, C_n, and D_n are assumed known. These equations are easily solved by the Thomas algorithm (ref. 26), which can be written as

$$\omega_{m,n} = D'_n + C'_n\omega_{m,n-1} \tag{24}$$

where

$$\left.\begin{aligned} D'_n &= \frac{D_n - C_nD'_{n+1}}{B_n + C_nC'_{n+1}} \\ C'_n &= -\frac{A_n}{B_n + C_nC'_{n+1}} \end{aligned}\right\} \tag{25}$$

The quantities D'_n and C'_n are computed from the outer boundary to the wall with the outer boundary condition $\omega(\xi,\infty) = 0$ imposed by setting $D'_N = C'_N = 0$, where N denotes the grid point at the outer boundary. Equation (24) is then used to deduce $\omega_{m,n}$, provided the value at the wall $\omega_{m,1}$ is known. An implicit procedure for deducing the wall vorticity is described in the next section.

Calculation of wall vorticity.- The wall vorticity can either be estimated and later updated from the subsequent solution, or it can be found along with the column solution by simultaneously solving the stream-function equation (eq. (13)). The latter procedure was used in the present investigation.

Equation (13) can be evaluated to second-order accuracy at the point $\xi = m\,\Delta\xi$, $\eta = \left(n + \frac{1}{2}\right)\Delta\eta$ by

$$\frac{\tilde{\psi}_{m,n+1} - \tilde{\psi}_{m,n}}{\Delta\eta} = \delta_m^{*2}\left(1 - \eta_{n+\frac{1}{2}}\right)\frac{\omega_{m,n+1} + \omega_{m,n}}{2} \tag{26}$$

Equation (13) must be evaluated at a half-grid point above, and not below the level at which the vorticity equation (eq. (12)) is differenced so that the outer boundary condition $\tilde{\psi}(\xi,\infty) = 0$ enters the problem. Equation (26) can be combined with equation (24) to obtain a recurrence relation for the stream function which is given by

$$\tilde{\psi}_{m,n} = K_n + L_n\omega_{m,n-1} \tag{27}$$

where

$$\left.\begin{aligned} K_n &= K_{n+1} + E_n\left[D'_{n+1} + D'_n\left(1 + C'_{n+1}\right)\right] + D'_nL_{n+1} \\ L_n &= C'_n\left[L_{n+1} + E_n\left(1 + C'_{n+1}\right)\right] \\ E_n &= \frac{\Delta\eta}{2}\,\delta_m^{*2}\left(\eta_{n+\frac{1}{2}} - 1\right) \end{aligned}\right\} \tag{28}$$

The quantities K_n and L_n are computed from the outer boundary, to the wall, with the boundary conditions $\omega(\xi,\infty) = \tilde{\psi}(\xi,\infty) = 0$ imposed by setting $K_N = L_N = 0$. The wall vorticity $\omega_{m,1}$ is found by combining equation (26), which is evaluated at $\eta = \Delta\eta/2$ and in which the boundary condition $\tilde{\psi}(\xi,0) = 0$ is imposed, with equations (24) and (27) which are evaluated at $\eta = \Delta\eta$ (n = 2) to obtain

$$\omega_{m,1} = -\frac{\frac{\Delta\eta}{2}\,\delta_m^{*2}\left(1 - \frac{\Delta\eta}{2}\right)D'_2 - K_2}{\frac{\Delta\eta}{2}\,\delta_m^{*2}\left(1 - \frac{\Delta\eta}{2}\right)\left(C'_2 + 1\right) - L_2} \tag{29}$$

Using this result, equations (24) and (27) may now be used to compute $\omega_{m,n}$ and $\tilde{\psi}_{m,n}$ by back substituting from the wall to the outer boundary.

Stability considerations.- Several global iterative procedures for solving equations (17) and (26) were developed, but were found to be unstable in certain calculations, particularly as the magnitude of the streamwise gradients increased. However, these instabilities were eliminated by the introduction of a time-like term in equation (17) to establish unconditional diagonal dominance. In addition, the introduction of this term results in a global iterative scheme which can be analyzed for linear stability by the von Neumann analysis. Furthermore, it was necessary to use underrelaxation to obtain converged solutions. Denoting the unknown vorticity in equation (17) as W_n, these modifications can be described by rewriting equation (17) as

$$A_n W_{n-1} + (B_n + \alpha)W_n + C_n W_{n+1} = D_n + \alpha\omega^j_{m,n} \tag{30}$$

followed by the relaxation equation

$$\omega^{j+1}_{m,n} = \omega^j_{m,n} + r\left(W_n - \omega^j_{m,n}\right) \tag{31}$$

where the superscript j denotes the global iteration level and r is the relaxation factor. Thus W_n is a temporary value of the vorticity along the column currently being updated. Equation (27) for the stream function is modified to give

$$S_n = K_n + L_n W_{n-1} \tag{32}$$

with the relaxed value of the stream function found from

$$\tilde{\psi}^{j+1} = \tilde{\psi}^j + r\left(S_n - \tilde{\psi}^j_{m,n}\right) \tag{33}$$

Expressions for α for forward and reversed flow are determined so that diagonal dominance is maintained; that is,

$$\left|B_n + \alpha\right| \geqq \left|A_n\right| + \left|C_n\right| \tag{34}$$

even if $C_\xi = 0$, and these expressions are given by

$$\left.\begin{aligned} u \geqq 0 \qquad & \alpha = \left|C_\eta\right| \\ u < 0 \qquad & \alpha = 2\left|C_\eta\right| \end{aligned}\right\} \tag{35}$$

where C_η is determined by equation (20) or (23) depending on whether the flow is forward or reversed. These values of α insure that if equation (34) is satisfied, then, as shown inductively by Keller (ref. 27), $\left|C_n'\right| \leqq 1$, thereby insuring no growth of round-off errors in applying equation (24). In the present calculations, modified expressions for α were used such that $\left|L_n\right| \leqq 1$ as well as $\left|C_n'\right| \leqq 1$. These relationships are found to be

$$\left.\begin{aligned} u \geqq 0 \qquad & \alpha = \left|C_\eta\right| + \left|1 + C_\eta\right|\left|E_n\right| \\ u < 0 \qquad & \alpha = 2\left(\left|C_\eta\right| + \left|1 + C_\eta\right|\left|E_n\right|\right) \end{aligned}\right\} \tag{36}$$

where, as before, C_η is determined by either equation (20) or (23); E_n is given in equation (28).

The linear stability of the finite-difference forms of the vorticity-transport equation is examined with the von Neumann analysis in appendix A. Both forward and reversed flow are considered. A stability analysis of the stream-function computation is considered unnecessary. The stream-function calculation, despite the complications introduced by the implicit treatment of the wall vorticity, is simply an integral of the vorticity across the boundary layer and should be stable (provided the vorticity computation is stable). The stability analysis of the vorticity computation is begun by eliminating the temporary value W_n between equations (30) and (31). The elimination results in

$$A_n\omega_{m,n-1}^{j+1} + (B_n + \alpha)\omega_{m,n}^{j+1} + C_n\omega_{m,n+1}^{j+1} = rD_n + \alpha\omega_{m,n}^{j} + (1 - r)\left(A_n\omega_{m,n-1}^{j} + B_n\omega_{m,n}^{j} + C_n\omega_{m,n+1}^{j}\right) \tag{37}$$

In appendix A the details of the von Neumann analysis of equation (37) are presented. This analysis shows that as $\Delta\xi,\ \Delta\eta \to 0$, with $\Delta\eta^2/\Delta\xi$ held constant to preserve the highest ξ and η derivatives, the only restriction for either forward or reversed flow is that $r \leqq 1$. In this limit the lower order derivatives are suppressed by the zero grid size; the remaining terms form the relaxation solution of the diffusion equation

$$\frac{\partial\omega}{\partial\xi} = \sigma\frac{\partial^2\omega}{\partial\eta^2} \tag{38}$$

where σ is the diffusion coefficient. Thus, with the present schemes the diffusion equation cannot be overrelaxed.

For finite grid size the inclusion of the lower order terms has no effect on the first-order scheme used in reversed flow. However, for forward flow it is found that the lower order terms may be destabilizing, and thus may impose a limit on the maximum size of the grid spacings which can be used. This point is further discussed in appendix A along with a discussion of some numerical results which qualitatively confirm the stability analysis. However, it appears from the calculations that the grid size used in the present study is sufficiently small to suppress the adverse stability effects of the lower order terms. Hence, other than the restriction of underrelaxation, the calculations presented in this report were performed with no grid constraints other than that of truncation errors. The effect of the lower order terms in the present investigation is the same as that discussed by Richtmyer and Morton (ref. 28) in that, for diffusion problems, the stability criterion is essentially unaltered by the inclusion of the lower order terms for a wide range of finite-difference schemes.

An alternate scheme for forward flow with second-order accuracy is also presented in appendix A. In this scheme, the destabilizing influence of the lower order terms is eliminated when no underrelaxation is used; that is, when $r = 1$. This scheme was described previously in reference 19 as having unconditional stability by the von Neumann analysis. This condition is now shown to be true only when no relaxation is used. However, underrelaxation was generally used in the present calculations; thus, this alternate scheme is of little value. The value of the relaxation factor typically used in the present study is between 0.4 and 1.0. A short discussion based on some numerical results is given in appendix A in which it is suggested that underrelaxation is required primarily so that the computation of the surface vorticity is stabilized.

Computation procedure.- The global iterative procedure is initialized by guessing the values of ω and $\tilde{\psi}$ at each point in the computational region (fig. 1). At the upstream boundary, the boundary conditions for ω and $\tilde{\psi}$ are prescribed. At the downstream boundary, it is assumed that the flow is attached; hence, it is unnecessary to impose any conditions here. The new iteration values of ω and $\tilde{\psi}$ are computed from equations (31) and (33), respectively, along the column of grid points from the wall to the outer boundary. In this computation, the most recently updated values of ω, $\tilde{\psi}$, and u have been used in evaluating the coefficients. The columns are computed successively beginning at the upstream boundary and continuing to some point downstream of reattachment. Since the flow is reversed and since an artificial time term has been introduced in the vorticity equation in order to maintain diagonal dominance, this sweep procedure from the upstream to the downstream boundary must be repeated iteratively. This global iterative process is continued until the following convergence criterion is satisfied:

$$\max_{m,n} \left| f_{m,n}^{j+1} - f_{m,n}^{j} \right| \leq 10^{-5} \tag{39}$$

where f represents ω, $\tilde{\psi}$, or u, that is, whichever quantity results in the largest residual.

Forward-Marching Procedure

In cases in which the velocity in the reversed flow region is small (5 percent or less of the free-stream velocity), the global iteration procedure described in the previous section is unnecessary. In these cases neglect of the streamwise convection in the reversed flow region should have only a slight influence on the resulting solution. For example, Reyhner and Flügge-Lotz (ref. 22) demonstrated that, by setting the convection term $u\frac{\partial u}{\partial x}$ in the x momentum equation equal to zero for u less than zero, a stable finite-difference solution of the boundary-layer equations could be obtained with the usual forward-marching procedure for a separated flow. This approximation eliminates the well-known instability encountered in solving the boundary-layer equations in a direction opposite to that of the local flow. The approximation also results in a substantial reduction in computer time and storage as compared to that required for a global iteration procedure. Several investigators (Dwoyer (ref. 2), Werle, Polak, and Berthe (ref. 23), and, more recently, Williams (ref. 24)) have used the Reyhner and Flügge-Lotz approximation in their separated boundary-layer calculations. An approximation similar to that of Reyhner and Flügge-Lotz (discussed by Carter and Wornom in ref. 20) is made in the present formulation by neglecting the streamwise convection of vorticity in the reversed flow region. Thus, when $u < 0$, set $u\delta^{*2}\frac{\partial \omega}{\partial \xi} = 0$; this approximation is implemented by setting $C_\xi = 0$.

With the inclusion of this approximation, the global iteration technique becomes the usual forward-marching procedure with column iteration which is typically used to solve the boundary-layer equations for an attached flow. Instabilities encountered in these calculations were eliminated by introducing time-like terms in the finite-difference equations, similar to those terms used in the global procedure. The introduction of these terms provides both unconditional diagonal dominance and a column iterative scheme which was found to be stable using the von Neumann stability analysis. In some cases Reyhner and Flügge-Lotz (also Werle, Polak, and Bertke (ref. 23) in a similar investigation) encountered an unexplained instability in the reverse flow region; they eliminated this instability by introducing a positive artificial convection term. Since this term increases the magnitude of the diagonal coefficients in the tridiagonal system of equations, it is possible that the instability in their solutions was caused by large errors in the Thomas algorithm because of a lack of diagonal dominance.

The approximate forward-marching technique with column iteration is somewhat similar to the global iterative procedure. Unconditional diagonal dominance is established by introducing a time-like term in equation (17) to give

$$A_n{}^q W_{n-1} + (B_n + \alpha)^q W_n + C_n{}^q W_{n+1} = D_n{}^q + (\alpha\omega_{m,n})^q \tag{40}$$

where q denotes the column iteration level. The value of α which was used in the calculations is given by equation (36) for $u \geqq 0$. Underrelaxation was used between repeated column iterations and is written as

$$\omega_{m,n}^{q+1} = \omega_{m,n}^{q} + r\left(W_n - \omega_{m,n}^{q}\right) \tag{41}$$

This modification of the finite-difference equations to obtain diagonal dominance results in a column iterative procedure which may be approximately analyzed by the von Neumann analysis. As in the global iterative procedure, the temporary value W_n is eliminated between equations (40) and (41) to give

$$A_n{}^q \omega_{m,n-1}^{q+1} + \left(B_n + \alpha\right)^q \omega_{m,n}^{q+1} + C_n{}^q \omega_{m,n+1}^{q+1} = rD_n{}^q + (\alpha\omega_{m,n})^q + (1 - r)\left(A_n{}^q \omega_{m,n-1}^{q} + B_n{}^q \omega_{m,n}^{q} + C_n{}^q \omega_{m,n}^{q}\right) \tag{42}$$

The substitution of a single Fourier component of arbitrary wave number k,

$$\omega_n{}^q = \omega_0{}^q e^{ik\eta}$$

into equation (42), where ω_0 is the amplitude, results in the amplification factor

$$\left|g\right| = \left|\frac{\omega_0^{q+1}}{\omega_0{}^q}\right| = \frac{\left|\alpha + (1 - r)\left(1 - \cos\phi + 2C_\xi\right) + i(1 - r)C_\eta \sin\phi\right|}{\left|\alpha + 1 - \cos\phi + 2C_\xi + iC_\eta \sin\phi\right|} \tag{43}$$

where $\phi = k\,\Delta\eta$ and $i = \sqrt{-1}$. The derivation of equation (43) is simplified by assuming $D_n{}^q$ is a constant. Since $D_n{}^q$ depends on A_n, C_n, and so on, which are assumed to be constant, it is neglected in the stability analysis. The von Neumann condition for stability is that $\left|g\right| \leqq 1$. Since $C_\xi \geqq 0$ and $\alpha \geqq 0$, this condition is satisfied in equation (43) if $r \leqq 1$. Thus, the repeated column iterations have linear stability provided that overrelaxation is not used; the same result was obtained previously for the global iterative procedure. This technique for obtaining unconditional diagonal dominance and column stability

is general, and should be applicable to other implicit finite-difference schemes such as the alternating direction implicit (ADI) solution procedure for solving the Navier-Stokes equations.

PRESCRIBED WALL-SHEAR FORMULATION

Governing Equations and Boundary Conditions

Three formulations of the boundary-layer equations for a prescribed wall shear are given below. The first formulation was given in reference 19; in certain calculations it resulted in a solution which varied discontinuously in the x-direction at a particular x location. More recently it has been found that this discontinuity can be eliminated by introducing a constraint on the edge velocity u_e, which is described in the second formulation.

The third formulation is a vorticity—stream-function equivalent of Klineberg and Steger's (ref. 9) formulation of the boundary-layer equations. The third formulation is expressed in primitive variables u and v. In one of Klineberg and Steger's calculations, an unexplained discontinuity occurred in the pressure-gradient parameter $\hat{m} = \frac{x}{u_e}\frac{du_e}{dx}$, which appears explicitly in their governing equations. In reference 19 it was conjectured that the two discontinuities mentioned might be related. This report shows that there is no relationship; hence, the discontinuity encountered by Klineberg and Steger remains unexplained. In an attempt to understand this discontinuity further, this case was recomputed using the present solution technique. However, in order to specify the same transformed wall-shear distribution as Klineberg and Steger, it was necessary to develop a new vorticity—stream-function formulation (designated as formulation 3).

Formulation 1 (ω, $\tilde{\psi}$, u).- The boundary-layer problem with the wall shear prescribed can be formulated in an analogous manner to that with the displacement thickness prescribed. In contrast to the primitive variables used by Klineberg and Steger (ref. 9), the use of vorticity as a dependent variable seems particularly simple for a prescribed wall shear since Dirichlet boundary conditions on the vorticity are imposed at both the wall and boundary-layer edge. The governing equations and boundary conditions for a prescribed wall-shear distribution $\omega_0(\xi)$ can be written as follows, where the displacement thickness (now unknown) has been replaced in equations (12) and (13) by a given scaling function $f(x)$,

$$uf^2 \frac{\partial \omega}{\partial \xi} - f \frac{\partial}{\partial \xi}\left[\tilde{\psi} + (\eta - 1)(uf)\right]\frac{\partial \omega}{\partial \eta} = \frac{\partial^2 \omega}{\partial \eta^2} \tag{44}$$

$$\frac{\partial \tilde{\psi}}{\partial \eta} = f^2(1 - \eta)\omega \tag{45}$$

$$\left.\begin{aligned} u(\xi,0) &= \tilde{\psi}(\xi,0) = 0 \\ \omega(\xi,0) &= \omega_0(\xi) \end{aligned}\right\} \tag{46}$$

$$\omega(\xi,\eta) \to 0 \quad \text{as} \quad \eta \to \infty \tag{47}$$

where the independent variables are

$$\left.\begin{aligned} \xi &= x \\ \eta &= \frac{y}{f} \end{aligned}\right\} \tag{48}$$

and the transformed stream function is

$$\tilde{\psi} = \psi - uf(\eta - 1) \tag{49}$$

After the vorticity is deduced, u is given by

$$u(\xi,\eta) = f \int_0^\eta \omega(\xi,\eta_1)\, d\eta_1 \tag{50}$$

where the boundary condition $u(\xi,0) = 0$ has been imposed. In the present calculations the scaling function is chosen as $f(x) = \delta_0^* \sqrt{x/x_0}$ where δ_0^* is the displacement thickness at the upstream boundary located at x_0.

After the calculation is completed, the unknown edge velocity may be deduced from the velocity profile given by equation (50) with $\eta = \infty$ or from the x momentum equation evaluated at $\eta = 0$ which gives

$$u_e \frac{du_e}{d\xi} = -\frac{1}{f} \left.\frac{\partial \omega}{\partial \eta}\right|_{\eta=0} \tag{51}$$

The edge velocity is deduced from equation (51) by integrating from the upstream boundary where u_e is known. The value of u_e (referred to as the profile value) deduced from equation (50) and that value deduced from equation (51) should agree; in fact, this redundancy serves as a useful check on the solution accuracy. For those solutions in

which discontinuities occurred, it was found that the u_e from the profile was discontinuous; that value deduced from equation (51) was not. Therefore, this discontinuity was eliminated by forcing these two u_e values to be equal. This step results in the modified formulation presented in the following section.

Formulation 2 (ω, ψ, u; u_e).- The transformed stream function is replaced with the usual stream function in equation (44), and the vorticity-transport equation is then written as

$$f\left(\frac{\partial\psi}{\partial\eta}\frac{\partial\omega}{\partial\xi} - \frac{\partial\psi}{\partial\xi}\frac{\partial\omega}{\partial\eta}\right) = \frac{\partial^2\omega}{\partial\eta^2} \tag{52}$$

subject to the boundary conditions

$$\omega(\xi,0) = \omega_o(\xi) \tag{53}$$

$$\omega(\xi,\eta) \to 0 \quad \text{as} \quad \eta \to \infty \tag{54}$$

After the vorticity is deduced, the u component of velocity is found from the solution of

$$\frac{\partial^2 u}{\partial\eta^2} = f\frac{\partial\omega}{\partial\eta} \tag{55}$$

Equation (55) is obtained by differentiating the definition of vorticity $\omega = \frac{1}{f}\frac{\partial u}{\partial\eta}$ with respect to η. It is convenient to solve this second-order equation for the velocity in order to impose simultaneously both of the following boundary conditions:

$$u(\xi,0) = 0 \tag{56}$$

and

$$u(\xi,\eta) \to u_e(\xi) = \left[u_e^2(\xi_o) - 2\int_{\xi_o}^{\xi}\frac{1}{f}\omega_\eta(\xi_1,0)\,d\xi_1\right]^{1/2} \quad \text{as} \quad \eta \to \infty \tag{57}$$

The latter of these conditions is the integral of equation (51) where ξ_o is the position of the upstream boundary. The stream function is then given by

$$\psi(\xi,\eta) = f\int_0^{\eta} u(\xi,\eta_1)\,d\eta_1 \tag{58}$$

where the boundary condition $\psi(\xi,0) = 0$ has been imposed.

In order for equation (57) to be satisfied, the vorticity must vanish at large distances from the surface. Thus, the imposition of equation (57) automatically insures that equation (54) is satisfied. Hence, the main difference between the two formulations given herein is that, in the second, a stronger outer boundary condition is imposed by constraining u_e as well as imposing a zero value of vorticity at the boundary-layer edge. In the first formulation, only the latter boundary condition is imposed.

Formulation 3 ($\hat{\tau}$, $\hat{\psi}$, $\hat{u}$; $\hat{m}$).- Klineberg and Steger (ref. 9) solved the following boundary-layer equations

$$x\frac{\partial\hat{u}}{\partial x} + \frac{\partial\hat{v}}{\partial\hat{y}} + \frac{\hat{m}+1}{2}\hat{u} = 0 \tag{59}$$

and

$$x\hat{u}\frac{\partial\hat{u}}{\partial x} + \hat{v}\frac{\partial\hat{u}}{\partial\hat{y}} = \hat{m}(1-\hat{u}^2) + \frac{\partial^2\hat{u}}{\partial\hat{y}^2} \tag{60}$$

where

$$\left.\begin{aligned} \hat{y} &= y\sqrt{\frac{u_e}{x}} \\ \hat{u} &= \frac{u}{u_e} \\ \hat{v} &= v\sqrt{\frac{x}{u_e}} + \frac{\hat{m}-1}{2}\hat{y}\hat{u} \\ \hat{m} &= \frac{x}{u_e}\frac{du_e}{dx} \end{aligned}\right\} \tag{61}$$

Klineberg and Steger solved these equations subject to the boundary conditions

$$\hat{y} = 0 \qquad \hat{u} = \hat{v} = 0 \qquad \frac{\partial\hat{u}}{\partial\hat{y}} = \hat{\tau}_0(x) \tag{62}$$

$$\hat{y} \to \infty \qquad \hat{u} \to 1 \tag{63}$$

where $\hat{\tau}_0(x)$ is a prescribed function. The pressure-gradient parameter $\hat{m}$ is deduced from equation (60) evaluated at $\hat{y} = 0$; this step gives

$$\hat{m} = -\frac{\partial^2\hat{u}}{\partial\hat{y}^2} \tag{64}$$

The transformed shear $\hat{\tau}$ is related to usual vorticity ω by

$$\hat{\tau} = \sqrt{\frac{x}{u_e}} \frac{1}{u_e} \omega \tag{65}$$

which involves the unknown edge velocity. Therefore, in order to compute the same case as Klineberg and Steger (ref. 9) with the present technique, it is necessary to write the vorticity equation in terms of the transformed shear $\hat{\tau}$. This step is easily done by differentiating equation (60) with respect to $\hat{y}$. The differentiation gives

$$x \frac{\partial \hat{\psi}}{\partial \hat{y}} \frac{\partial \hat{\tau}}{\partial x} - \left[\hat{\psi} \left(\frac{1 + \hat{m}}{2} \right) + x \frac{\partial \hat{\psi}}{\partial x} \right] \frac{\partial \hat{\tau}}{\partial \hat{y}} = \frac{\partial^2 \hat{\tau}}{\partial \hat{y}^2} - \hat{\tau} \frac{\partial \hat{\psi}}{\partial \hat{y}} \left(\frac{3\hat{m} - 1}{2} \right) \tag{66}$$

where the stream function $\hat{\psi}$ has been introduced as

$$\left.\begin{aligned} \hat{u} &= \frac{\partial \hat{\psi}}{\partial \hat{y}} \\ \hat{v} &= -\frac{\hat{\psi}}{2}(1 + \hat{m}) - x \frac{\partial \hat{\psi}}{\partial x} \end{aligned}\right\} \tag{67}$$

Equation (67) automatically insures that the continuity equation is satisfied. The transformed shear is determined from equation (66) subject to the boundary conditions

$$\hat{\tau}(x,0) = \hat{\tau}_o(x) \tag{68}$$

$$\hat{\tau}(x,\hat{y}) \to 0 \quad \text{as} \quad \hat{y} \to \infty \tag{69}$$

The remainder of the formulation closely follows that given in formulation 2. After the transformed shear is deduced, the $\hat{u}$ component of velocity is found from

$$\frac{\partial^2 \hat{u}}{\partial \hat{y}^2} = \frac{\partial \hat{\tau}}{\partial \hat{y}} \tag{70}$$

subject to the boundary conditions

$$\hat{u}(x,0) = 0 \tag{71}$$

$$\hat{u}(x,\hat{y}) \to 1 \quad \text{as} \quad \hat{y} \to \infty \tag{72}$$

The stream function is then given by

$$\hat{\psi}(x,\hat{y}) = \int_0^{\hat{y}} \hat{u}\left(x,\hat{y}_1\right) d\hat{y}_1 \tag{73}$$

where the boundary condition $\hat{\psi}(x,0) = 0$ has been imposed. The pressure-gradient parameter is then found from

$$\hat{m}(x) = -\frac{\partial \hat{\tau}}{\partial \hat{y}}\bigg|_{\hat{y}=0} \tag{74}$$

Numerical Technique

Formulation 1.- The finite-difference form of equations (44) and (45) is solved with a global iteration procedure similar to that presented for the prescribed displacement thickness formulation. However, in the forward flow regions, the Crank-Nicholson scheme produced small streamwise oscillations which were eliminated by use of the computational molecule shown in figure 1. In this case the ξ derivatives are represented to second-order accuracy by a three-point backward-difference expression; the η derivatives in the vorticity equation are represented by the usual central-difference expressions. In the reversed flow region, the finite-difference representation of the vorticity equation is the same as that used for the prescribed displacement thickness approach.

In both the forward and reversed flow regions, the finite-difference representation of equation (44) can be written in the form of equation (30) where, if the flow is forward

$$\left.\begin{aligned} A_n &= -\left(C_\eta + 1\right) \\ B_n + \alpha &= 2 + 3C_\xi + 2\left|C_\eta\right| \\ C_n &= C_\eta - 1 \\ D_n + \alpha\omega^j_{m,n} &= C_\xi\left(4\omega^{j+1}_{m-1,n} - \omega^{j+1}_{m-2,n}\right) + 2\left|C_\eta\right|\omega^j_{m,n} \end{aligned}\right\} \tag{75}$$

and

$$\left.\begin{aligned} C_\xi &= \frac{\Delta\eta^2}{2\,\Delta\xi}\left(uf^2\right)_{m,n} \\ C_\eta &= -\frac{\Delta\eta}{2}\left\{f\,\frac{\partial}{\partial\xi}\left[\tilde{\psi} + (\eta - 1)(uf)\right]\right\}\Bigg|_{m,n} \end{aligned}\right\} \tag{76}$$

Three-point backward-difference expressions are used for the ξ derivatives in equation (76). If the flow is reversed

$$\left.\begin{aligned} A_n &= -\left(C_\eta + 1\right) \\ B_n + \alpha &= 2\left(1 - C_\xi + \left|C_\eta\right|\right) \\ C_n &= C_\eta - 1 \\ D_n + \alpha\omega^j_{m,n} &= -2C_\xi\omega^j_{m+1,n} + 2\left|C_\eta\right|\omega^j_{m,n} \end{aligned}\right\} \tag{77}$$

where C_ξ and C_η are given in equation (76). For reversed flow, central differences are used for the ξ derivatives in C_η.

The solution of equation (30) for the vorticity is again found with the Thomas algorithm. The Thomas algorithm is given in equations (24) and (25) subject to the boundary conditions of equations (46) and (47). The relaxation equation given in equation (31) is then used to compute the new vorticity value. The stream function is then found by computing

$$S_n = S_{n-1} + \Delta\eta f_m{}^2\left(1 - \eta_{n-\frac{1}{2}}\right)\frac{\omega^{j+1}_{m,n-1} + \omega^{j+1}_{m,n}}{2} \tag{78}$$

from the wall to the edge of the boundary layer with the relaxed value of the stream function computed from equation (33).

The linear stability of the global iterative scheme for the vorticity-transport equation is examined in appendix B for forward flow. For reversed flow the same scheme is used for the prescribed wall-shear calculations that is used for the prescribed displacement thickness calculations; this scheme is shown in appendix A to be stable for $r \leqq 1$. For forward flow, the analyses are also quite similar, since for $r \leqq 1$, the global iterative scheme is stable if the grid is refined to suppress the possible destabilizing influence of a lower order term. In practice, no instabilities which could be traced to a violation of the von Neumann condition were observed.

Formulations 2 and 3.- The numerical treatment of the vorticity-transport equation in these two formulations is the same as that used for formulation 1, with some minor changes. Small oscillations present in the solution of formulations 2 and 3 were eliminated by representing the term $\partial\psi/\partial\xi$ (or $\partial\hat{\psi}/\partial x$) by a combined first- and second-order difference expression which is given by

$$\left.\frac{\partial\psi}{\partial\xi}\right|_{m,n} = \beta\left(\frac{3\psi_{m,n} - 4\psi_{m-1,n} + \psi_{m-2,n}}{2\,\Delta\xi}\right) + (1 - \beta)\left(\frac{\psi_{m,n} - \psi_{m-1,n}}{\Delta\xi}\right) \tag{79}$$

where β is a weighting factor in the range of $0 \leqq \beta \leqq 1$. If $\beta = 1$, equation (79) has second-order accuracy; if $\beta = 0$, the equation has first-order accuracy. The value of β typically used was 0.8 or 0.9.

In contrast to equations (44) and (52), the transformed shear in formulation 3 appears undifferentiated in equation (66). In the finite-difference representation of equation (66), this term was treated implicitly. For example, equation (75) which is for forward flow becomes

$$B_n + \alpha = 2 + 3C_x + 2\left|C_y\right| + C_z \tag{80}$$

where

$$C_z = \Delta\eta^2 \hat{u}_{m,n}\left(\frac{3\hat{m}_m - 1}{2}\right) \tag{81}$$

and the definitions of C_x and C_y are analogous to those expressions for C_ξ and C_η given in equation (76).

In both formulations 2 and 3 the terms in equations (55) and (70) are represented by central differences and the resulting equations are solved for u (or $\hat{u}$) assuming ω (or $\hat{\tau}$) is known. The stream function is then deduced from equation (58) or (73) by using the trapezoidal rule.

In order to complete the solution at a given ξ station in formulation 2, equation (51) is solved to first order for u_e to give

$$u_{e,m}^{j+1} = u_{e,m}^{j} + r\left[u_{e,m-1}^{j+1} - \frac{\Delta\xi}{2\,\Delta\eta f_m u_{e,m}^{j}}\left(4\omega_{m,2}^{j+1} - \omega_{m,3}^{j+1} - 3\omega_{m,1}\right) - u_{e,m}^{j}\right] \tag{82}$$

where $\omega_{m,1} = \omega_o(\xi)$ which is the prescribed wall vorticity and r is the relaxation factor. The solution changed only slightly when equation (82) was modified to give second-order accuracy. In formulation 3 the pressure-gradient parameter $\hat{m}$ is deduced in a similar manner from

$$\hat{m}_m^{j+1} = \hat{m}_m^{j} + r\left[-\frac{1}{2\,\Delta\hat{y}}\left(4\hat{\tau}_{m,2}^{j+1} - \hat{\tau}_{m,3}^{j+1} - 3\hat{\tau}_o\right) - \hat{m}_m^{j}\right] \tag{83}$$

In both equations (82) and (83) the value of the relaxation factor used was typically 0.6, the same as that value used in solving for ω (or $\hat{\tau}$).

RESULTS AND DISCUSSION

Computational Rate

The computational rate on the CDC 6600 computer system for the results presented in this section is about 2300 grid points per second for the prescribed displacement thickness cases and about 3000 grid points per second for the prescribed wall-shear cases. In the global iterative procedure the number of iterations required for convergence is typically between 100 to 200; the prescribed initial conditions are the upstream boundary conditions repeated at each streamwise station. The computer time required for these calculations is usually 5 minutes or less, depending on the grid and the total number of iterations. In the prescribed displacement thickness procedure, the number of global iterations required for convergence was reduced considerably by using improved initial conditions obtained from the forward-marching procedure, which requires an average of 20 to 30 column iterations at each streamwise station.

Prescribed Displacement Thickness

Comparison with solutions of the Navier-Stokes equations.- Comparisons with Briley's (ref. 29) numerical solutions of the Navier-Stokes equations for the flow in the vicinity of a laminar separation bubble are presented. Figure 2 shows a schematic diagram of the computational region used by Briley in solving the vorticity—stream-function formulation of the Navier-Stokes equations. The outer boundary was located about four upstream boundary-layer thicknesses from the wall. Along this boundary, a linearly retarded boundary velocity u_b was prescribed, followed by a constant value. This boundary condition results in flow separation and reattachment as shown schematically in figure 2. Briley referred to this prescribed boundary velocity as u_e; however, in the present report u_e is the streamwise velocity component evaluated at the boundary-layer edge which is closer to the surface than the position of the outer boundary used by Briley. At the upstream boundary which was located at $x = 0.05$, Howarth's (ref. 30) solution of the boundary-layer equations was used for the boundary conditions. Briley discusses the fact that his solution of the Navier-Stokes equations does not account for the interaction of the viscous solution on the inviscid flow; likewise, the present boundary-layer approach has not been coupled to an inviscid calculation. Hence, both calculations can be regarded as the first stage of iteration with an inviscid flow. It is of interest to compare the resulting solutions in the viscous region. In the present calculation Howarth's solution is also used for the upstream boundary condition. The other boundary conditions are given in figure 1.

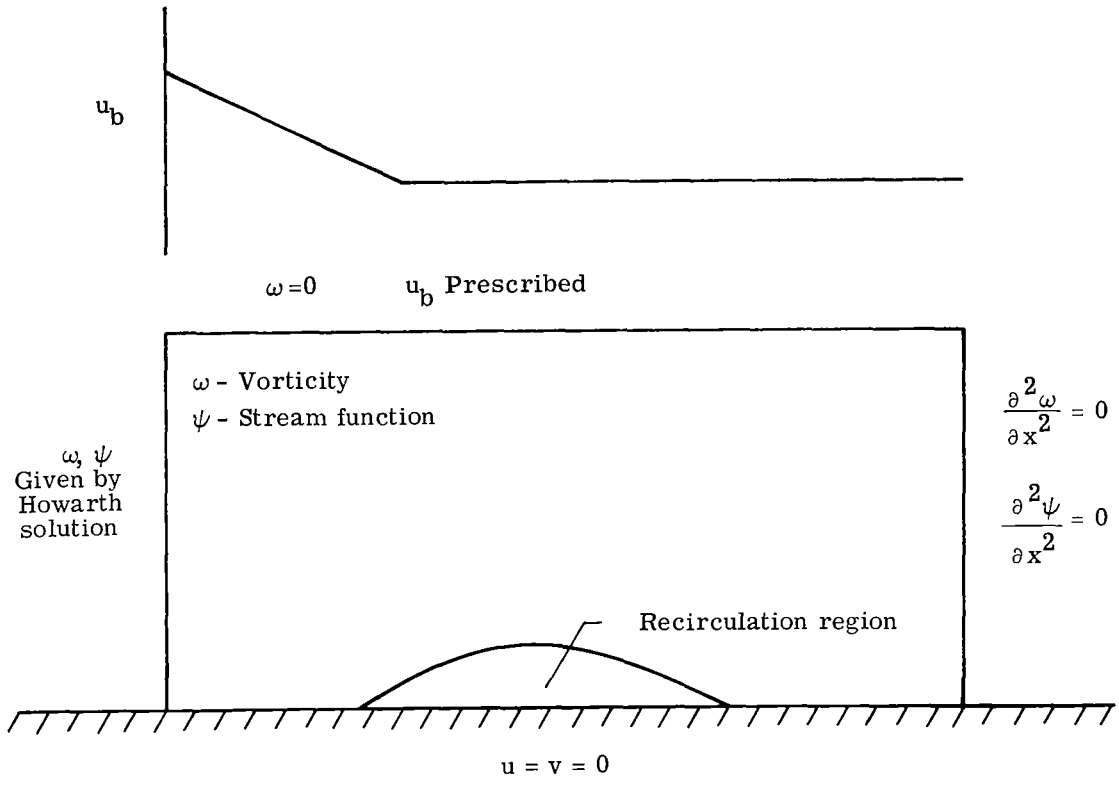

Figure 2.- Computational region used by Briley for Navier-Stokes equations.

In figures 3 and 4, the present results are compared with those obtained by Briley (solution 4 in ref. 29); in general, the agreement between the two solutions is excellent. The reference Reynolds number which Briley used is $R_{\infty,L} = 2.08 \times 10^4$. Figure 3 shows the displacement thickness deduced by Briley which is prescribed for the present calculations. A comparison of streamlines is given in figure 3 where $\psi\sqrt{R_{\infty,L}} = 0$ is the dividing streamline which separates the inner recirculating flow from the outer main flow. Figure 4 shows good agreement in the skin friction obtained by the two approaches. The skin-friction coefficient is related to the shear by $C_f\sqrt{R_{\infty,L}} = 2\overline{\omega}$. The grid spacings used in the present solution in figures 3 and 4 are $\Delta\xi = 0.00625$ and $\Delta\eta = 0.05$; only slight changes were observed in the solution when these values were doubled. On the fine grid, starting with crude initial conditions, the number of iterations required for convergence was 131; on the coarse grid, the number required was 106.

Figure 5(a) shows the boundary-layer edge velocity u_e deduced in the present calculation and the outer boundary velocity u_b prescribed by Briley. The agreement

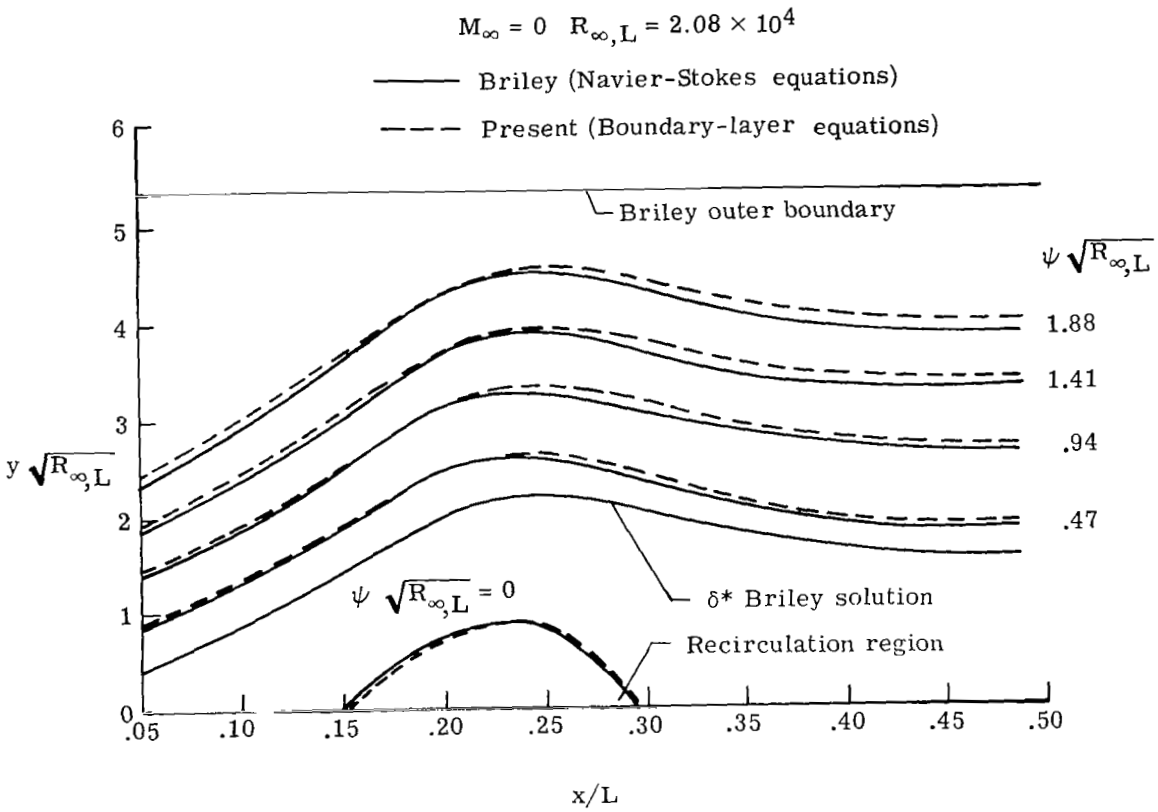

Figure 3.- Comparison of streamlines and recirculation region.

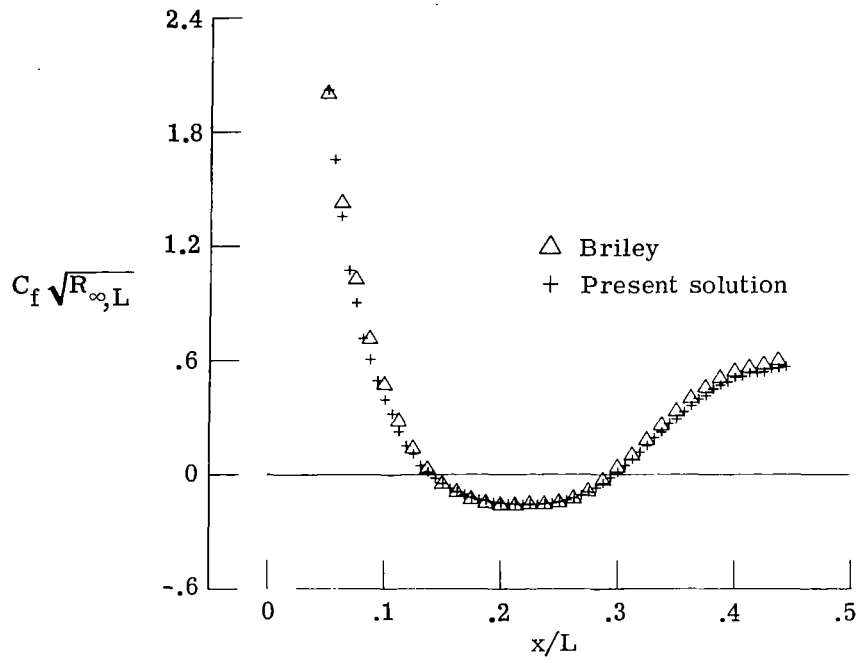

Figure 4.- Comparison of skin friction.

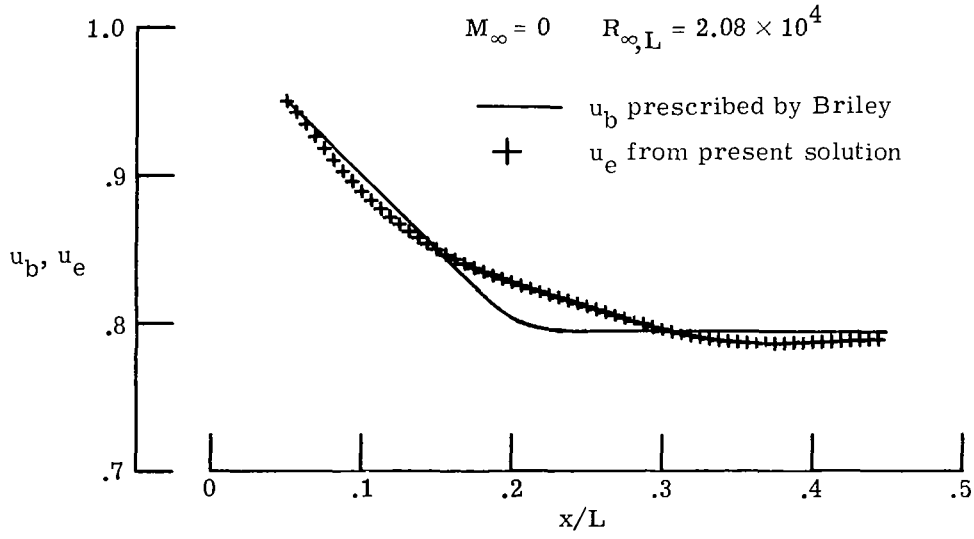

(a) Comparison of boundary and edge velocity.

Figure 5.- Velocity distributions and Meksyn pressure gradient parameter.

between the two distributions is relatively good. This good agreement suggests that the variation in the flow quantities between the boundary-layer edge and the outer boundary used by Briley is fairly small. However, according to Meksyn's (ref. 31) criterion, if u_e were exactly equal to u_b then the present boundary-layer solution would be singular at the separation point. From his approximate asymptotic method for the boundary-layer equations as well as from the experimental data of Schubauer (ref. 32) and others, Meksyn concluded that a necessary condition for a regular solution of the boundary-layer equations at separation is that the function

$$\lambda(x) = \left(\int_0^x u_e \, dx_1 \right) \frac{du_e}{dx} \frac{1}{u_e^2} \tag{84}$$

must have a local minimum prior to separation; hence, $\frac{d\lambda}{dx} > 0$ at $C_f = 0$. Figure 5(b) shows that the present solution satisfies this requirement; if the edge velocity were the same as Briley's boundary velocity, then the resulting λ does not. All solutions in the present investigation were found to satisfy Meksyn's criterion at the separation point. Klineberg and Steger found the same result in their calculations of separated flow, although they based their conclusions on the pressure-gradient parameter

$$\hat{m} = \frac{x}{u_e} \frac{du_e}{dx} \tag{85}$$

which is approximately equal to λ.

The calculation of the edge velocity serves as a check on the solution accuracy since, as noted in the prescribed wall-shear formulation, the edge velocity can be deduced either from the velocity profile or from the momentum equation evaluated at $\eta = 0$ resulting in

$$u_e \frac{du_e}{dx} = -\frac{1}{\delta^*} \frac{\partial \omega}{\partial \eta} \tag{86}$$

Knowing the wall-shear derivative and the value of u_e at the upstream boundary, equation (86) is integrated with respect to x (as given in eq. (57)) to obtain the u_e distribution. In the present computation of the Briley case, approximately a 10-percent difference in the two values of u_e was found at each x station when a first-order scheme was used for the calculation in the forward flow region. This difference was reduced to about 0.1 percent for the same grid when the second-order accurate Crank-Nicholson scheme was used. This result demonstrates the value of a second-order scheme in the forward flow region as it avoids the excessive number of grid points required to obtain an accurate solution with a first-order scheme.

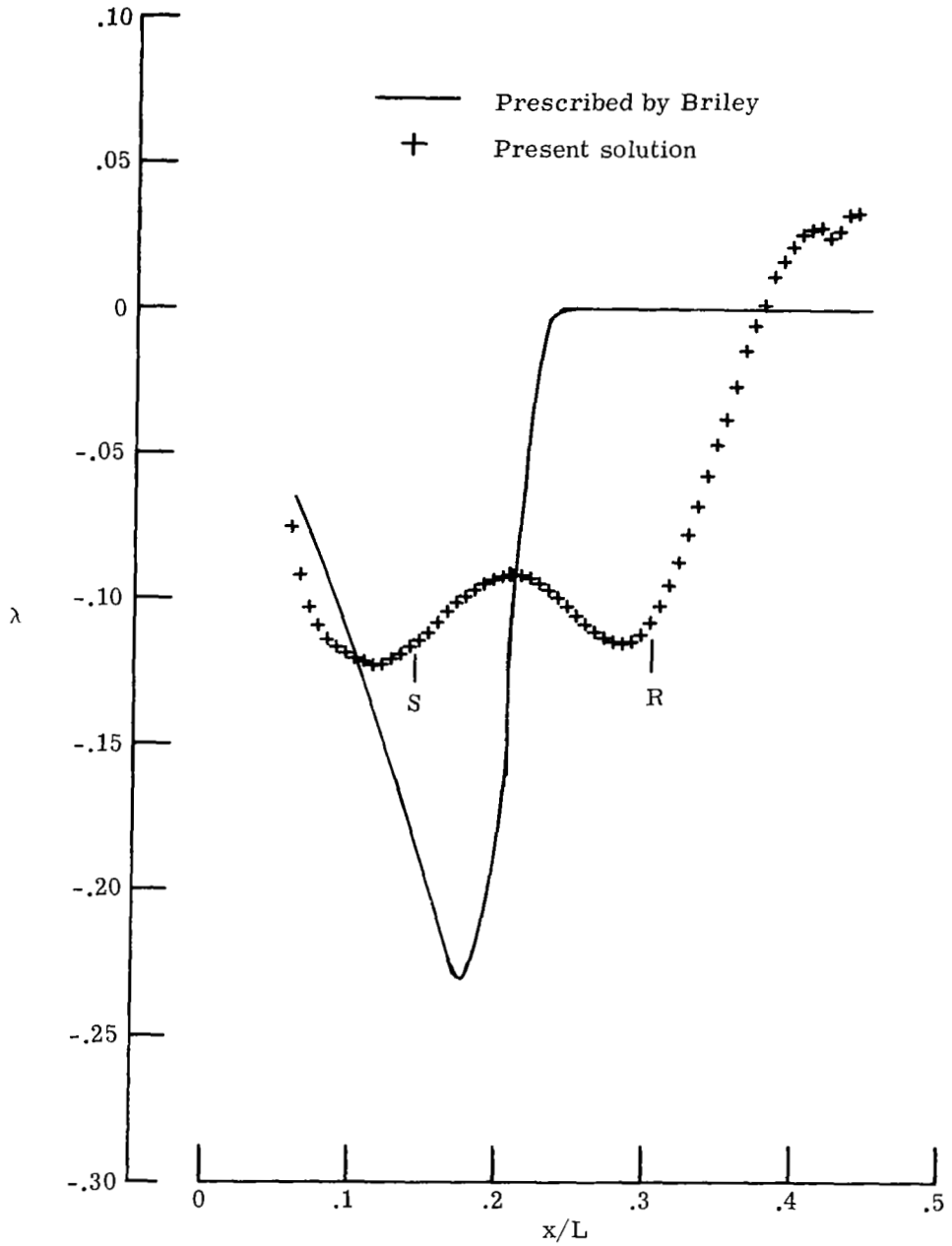

(b) Meksyn pressure-gradient parameter (S = Separation, R = Reattachment).

Figure 5.- Concluded.

Comparison with other boundary-layer solutions.- In this section a comparison between a solution obtained by Klineberg and Steger using a point iterative scheme for a prescribed wall shear and a solution using the present technique with δ^* prescribed is presented. The transformed wall shear prescribed by Klineberg and Steger is related to the usual vorticity in equation (65) and is given by

$$\hat{\tau}_o(x) = \frac{0.332}{12}(x - 2)(x - 6) = \hat{\tau}_1(x) \tag{87}$$

except for $2 \leqq x \leqq 6$ where

$$\hat{\tau}_o(x) = \hat{\tau}_1(x)\left[1 + \hat{\alpha}(x - 2)(x - 6)\right] \tag{88}$$

where $\hat{\alpha}$ is a given parameter. For $\hat{\alpha} = 0.1$, figure 6 shows the displacement thickness which they deduced for a typical separated flow calculation. The Blasius flat-plate displacement thickness is also shown in figure 6 for a basis of reference. If Klineberg and Steger's $\delta^*(x)$ is used as a prescribed condition and if their solution at $x = 1$ for the upstream boundary conditions is used the skin friction deduced in the present calculation

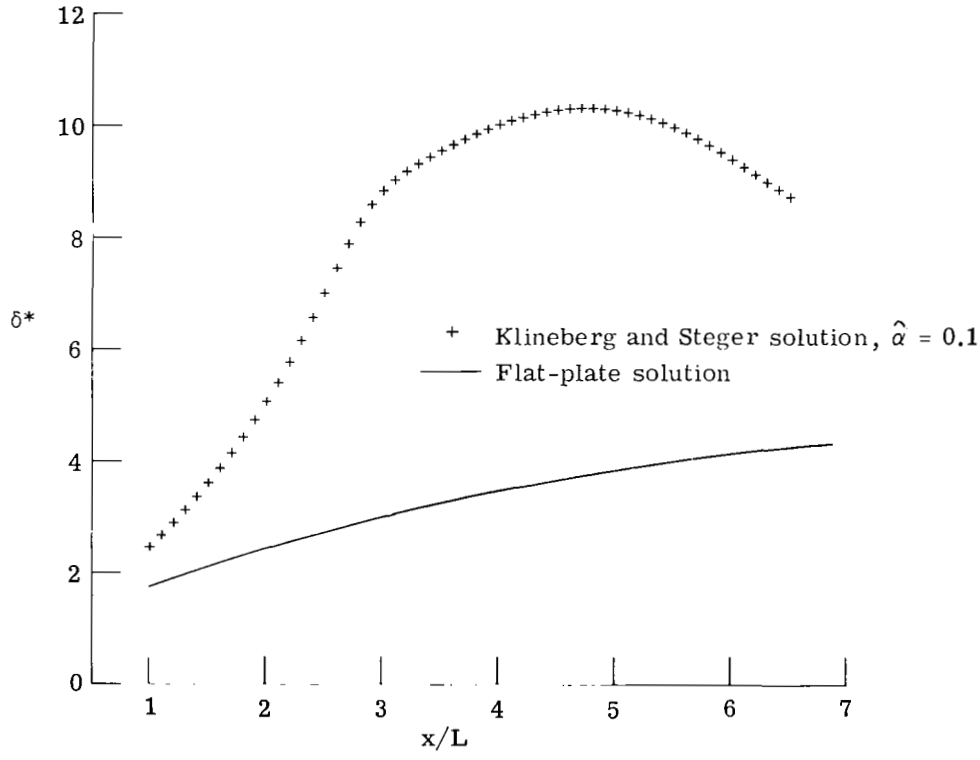

Figure 6.- Displacement thickness distributions.

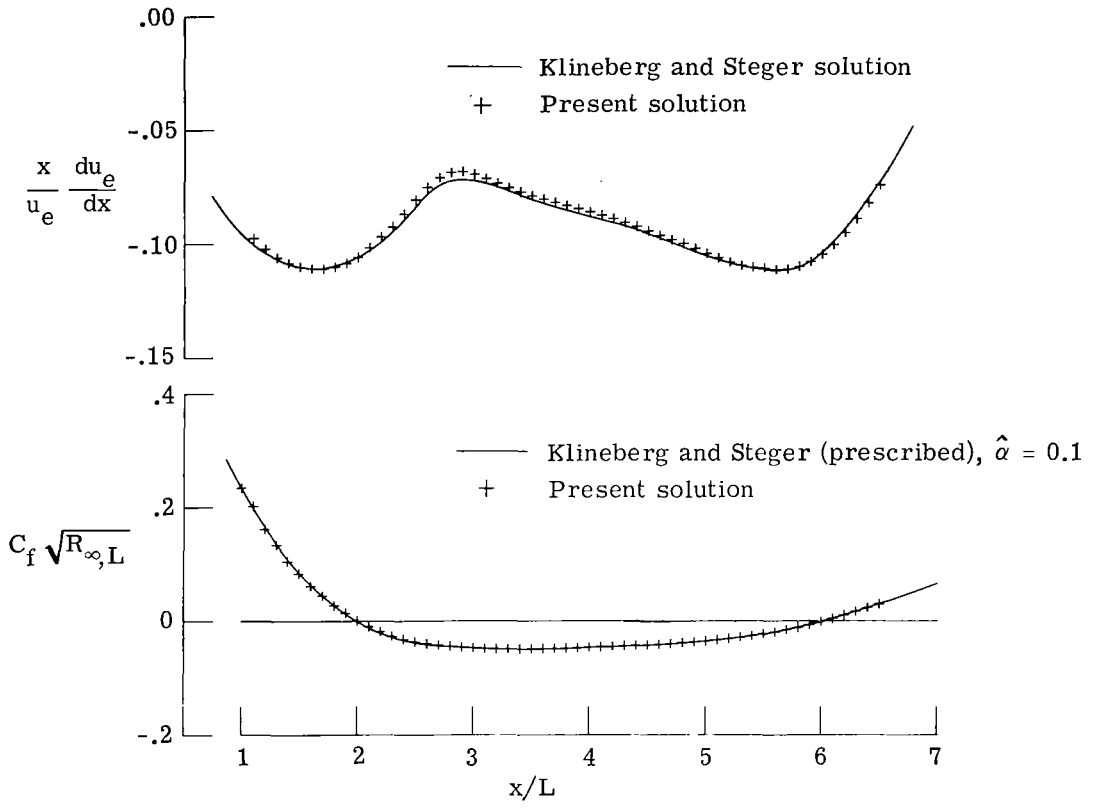

Figure 7.- Comparison of skin friction and pressure-gradient parameter.

is shown to be the same as that prescribed by Klineberg and Steger (fig. 7). Excellent agreement is also shown in figure 7 in comparing the pressure-gradient parameter $(x/u_e)du_e/dx$ obtained in the present solution with that found by Klineberg and Steger. The corresponding values of u_e agree to a few tenths of 1 percent. Profiles of the u component of velocity are plotted in figure 8 at several streamwise stations. No difference could be distinguished between these profiles and those obtained by Klineberg and Steger. Thus, at least for this case of separated flow, two inverse boundary-layer solution techniques which are significantly different produce essentially the same solution.

Using the same convergence criterion, this case of separated flow required 216 iterations for convergence in the present calculations as compared to approximately 850 required for convergence by Klineberg and Steger. This difference may be caused by the small underrelaxation factor (0.05) used by Klineberg and Steger on the pressure-gradient parameter in the early stages of iteration. No underrelaxation was needed for this case in the present calculations. The unknown edge velocity and the pressure gradient are eliminated from the present formulation; such elimination should increase the convergence rate caused by the sensitivity of the boundary-layer solution to the pressure gradient. In addition, the point iterative scheme may be slower since there is a delay in satisfying either

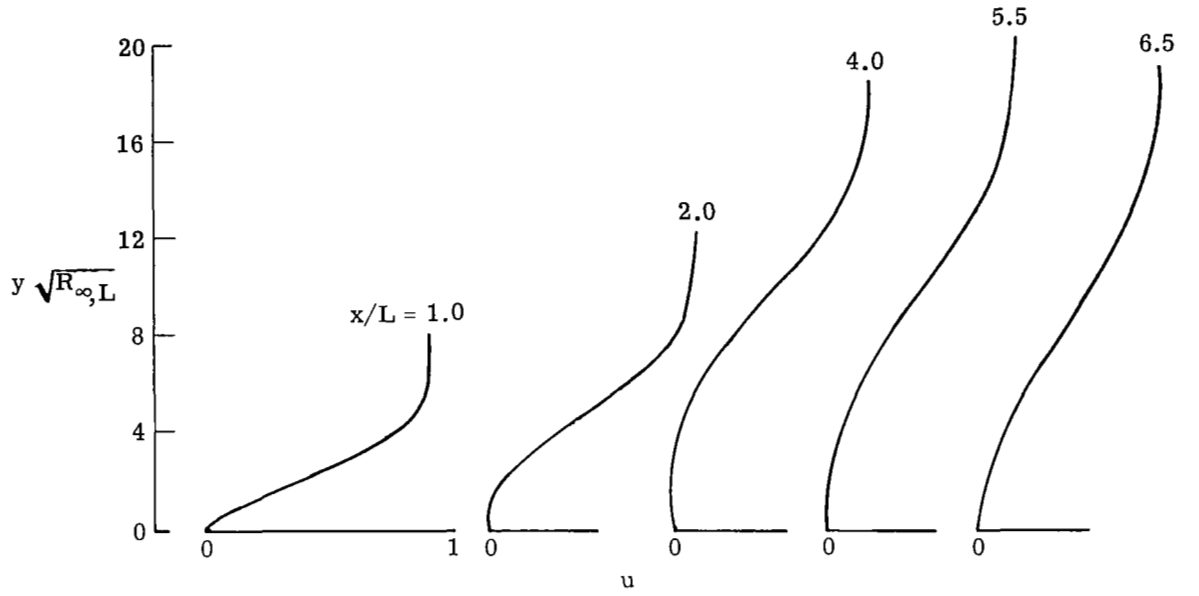

Figure 8.- Velocity profiles at several streamwise stations from present solution (δ^* prescribed).

the wall or the edge boundary condition, depending on the direction in which the solution is updated. In the column iterative scheme these boundary conditions are imposed simultaneously in updating the solution at each streamwise station. The above difference in the total number of iterations is partly compensated by the fact that the point iterative scheme requires less computer time per grid point than the column iterative procedure.

Additional calculations.- As a further test of the prescribed δ^* technique, additional calculations were performed in which the approach to separation was much more rapid and the reverse flow velocities were larger than in the Briley and Klineberg and Steger calculations. The prescribed δ^* used in these additional calculations for $\xi_0 \leqq \xi \leqq \xi_1$ is given by the cubic equation

$$\delta^*(\xi) = a_1 + a_2(\xi - \xi_0) + a_3(\xi - \xi_0)^2 + a_4(\xi - \xi_0)^3 \tag{89}$$

The constants a_1 to a_4 are determined so that, at $\xi = \xi_0$, the prescribed δ^* distribution matches the value and slope of the Blasius flat-plate distribution and, at $\xi = \xi_1, \delta^*$ reaches a maximum value. For $\xi_1 \leqq \xi \leqq \xi_2$, δ^* is given by a second cubic equation

$$\delta^*(\xi) = \bar{a}_1 + \bar{a}_2(\xi - \xi_1) + \bar{a}_3(\xi - \xi_1)^2 + \bar{a}_4(\xi - \xi_1)^3 \tag{90}$$

where $\bar{a}_1$ to $\bar{a}_4$ are determined by matching the first cubic at $\xi = \xi_1$. At $\xi = \xi_2$, δ^* becomes a minimum value $\delta_2{}^*$, which is generally chosen about the same as the Blasius

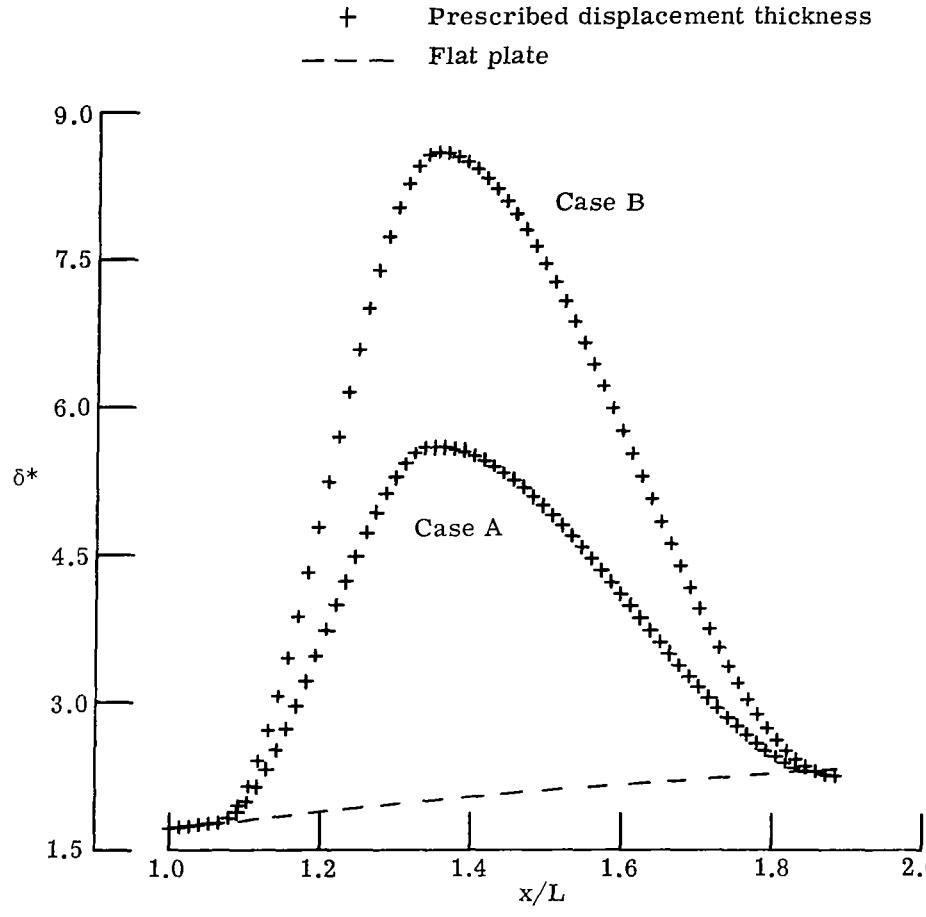

Figure 9.- Prescribed displacement thickness distributions.

flat-plate value at that particular ξ location. In figure 9, two δ^* distributions given by equations (89) and (90) are shown; in these equations, $\xi_0 = 1.065$, $\xi_1 = 1.35$, and $\xi_2 = 1.884$. The only difference between these two cases is that $\delta^*_{max} = 5.6$ in case A and $\delta^*_{max} = 8.6$ in case B. For these two cases $(d\delta^*/d\xi)_{max} = 20$ and $(d\delta^*/d\xi)_{max} = 36$ as compared to the values of 12 and 4.3 in the Briley and Klineberg and Steger calculations, respectively. The displacement thickness adds an angle to the given body shape by an amount $\frac{d\delta^*}{d\xi}\frac{1}{\sqrt{R_{\infty,L}}}$. For example, if $R_{\infty,L} = 10^5$, then in case B at the point of $(d\delta^*/d\xi)_{max}$ the effective body slope is increased by 6.5^o. For an aerodynamic shape such as an airfoil, a change in body slope of only a few degrees results in significant changes in the pressure distribution.

Figure 10 shows the streamline pattern in the shear layer and recirculation region for case A. The thickness of the reversed flow region is amplified here since the normal coordinate has been multiplied by the square root of the Reynolds number. This separa-

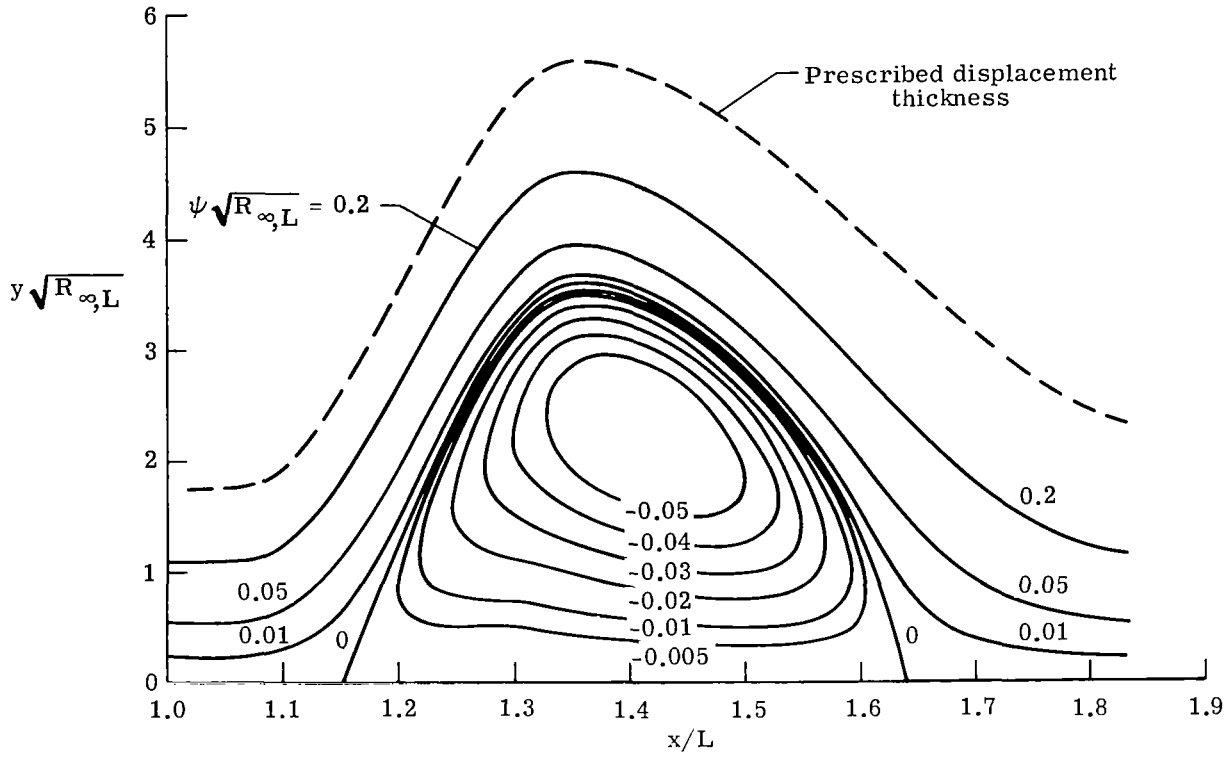

Figure 10.- Computed streamline pattern in separation bubble for case A.

tion bubble, which is typical of those calculated in the present investigation, is actually thin and is entirely confined to the interior of the viscous layer.

Figures 11 and 12 show the resulting solutions for the skin-friction, edge velocity, and pressure-gradient parameter λ for cases A and B, respectively. Only slight differences are observed in these calculations for the two different grid spacings which were used; hence, the present technique appears to yield accurate solutions on a relatively coarse grid. Comparison of the skin-friction distributions in figures 11(a) and 12(a) shows that in case B, because of the greater δ^*, the separated region is of greater extent than that in case A. The edge-velocity distributions for these two cases (figs. 11(b) and 12(b)) illustrate the usual variations found in a flow involving a significant amount of separation. Near the points of separation and reattachment, the edge velocity or pressure coefficient $C_p = 1 - \frac{u_e^2}{2}$ varies rapidly with an interim region of relatively constant pressure which is usually referred to as the pressure plateau region. The plateau region is better defined in case B since the separated region is larger.

In figures 11(c) and 12(c) it is seen that the pressure-gradient parameter λ given in equation (84) has a positive slope at separation and, hence, satisfies Meksyn's criterion for a regular solution at the separation point. In figures 11(c) and 12(c), as well as in

figures 5(b) and 7 for the Briley and Klineberg and Steger calculations, respectively, a second local minimum occurs in λ (or $\hat{m}$) just prior to reattachment. Similarly, in a recent investigation, Horton (ref. 13) presented a calculation for a prescribed wall shear in which Meksyn's criterion is satisfied at both separation and reattachment. These calculations provide further support for Meksyn's observation that the shape of the λ distribution is similar for a wide range of separated flows.

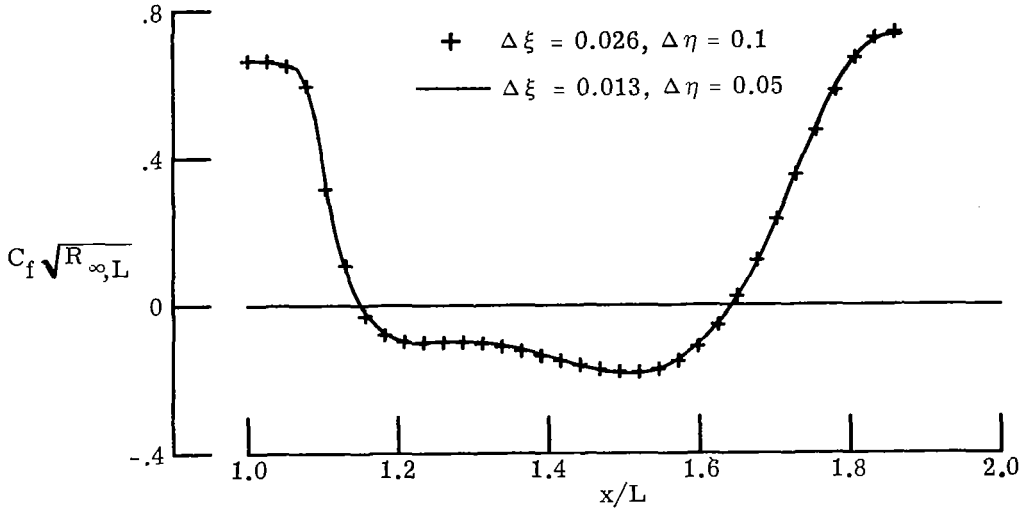

(a) Skin friction.

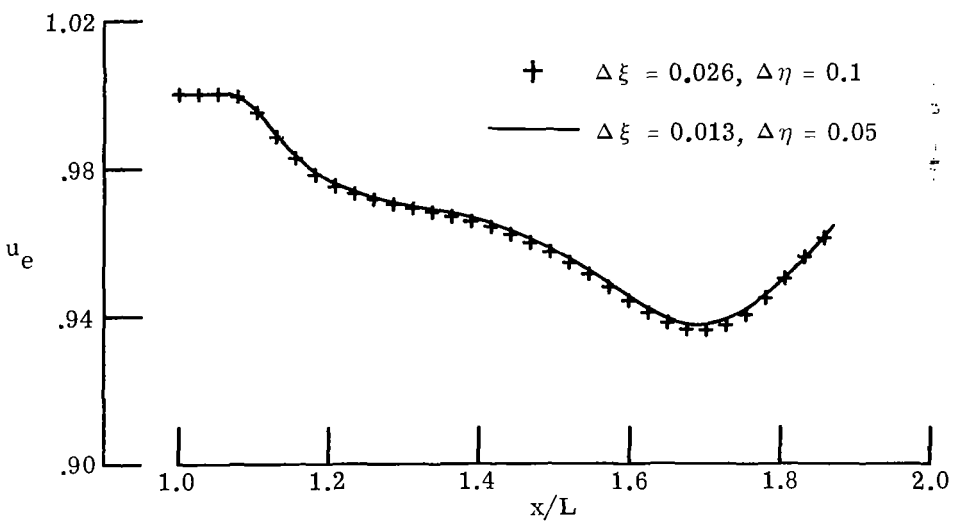

(b) Edge velocity.

Figure 11.- Effect of grid size on calculations for case A.

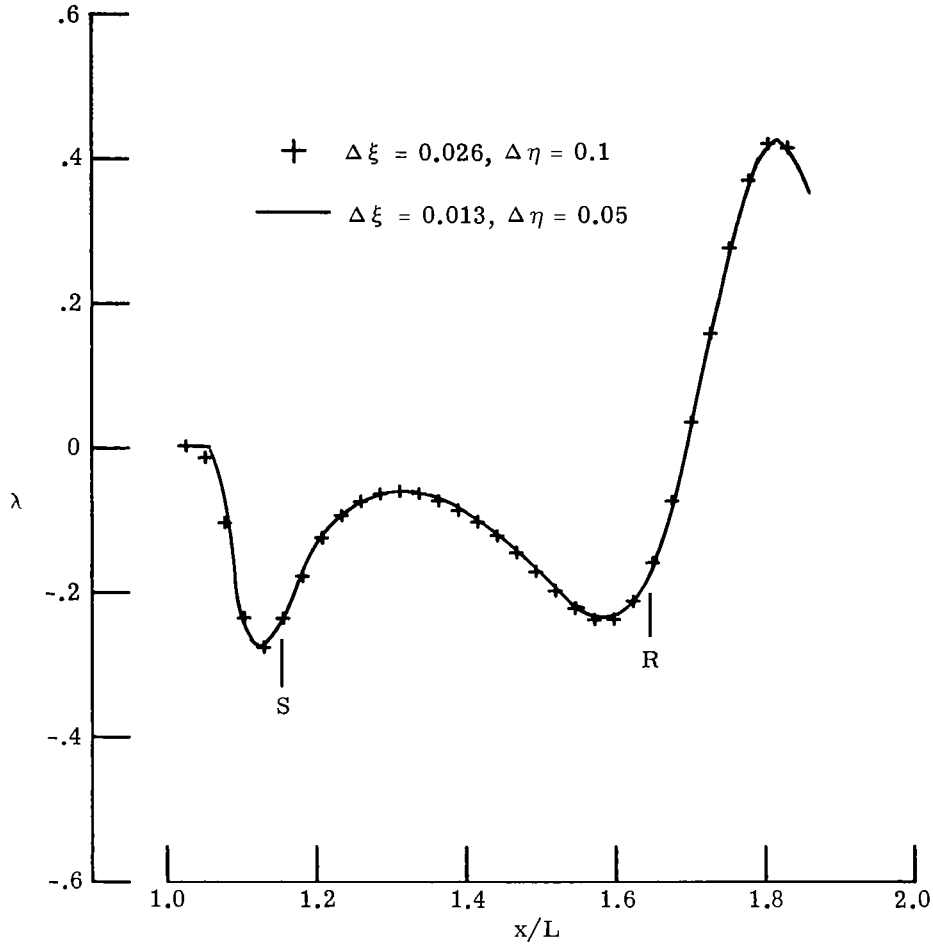

(c) Meksyn pressure-gradient parameter (S = Separation, R = Reattachment).

Figure 11.- Concluded.

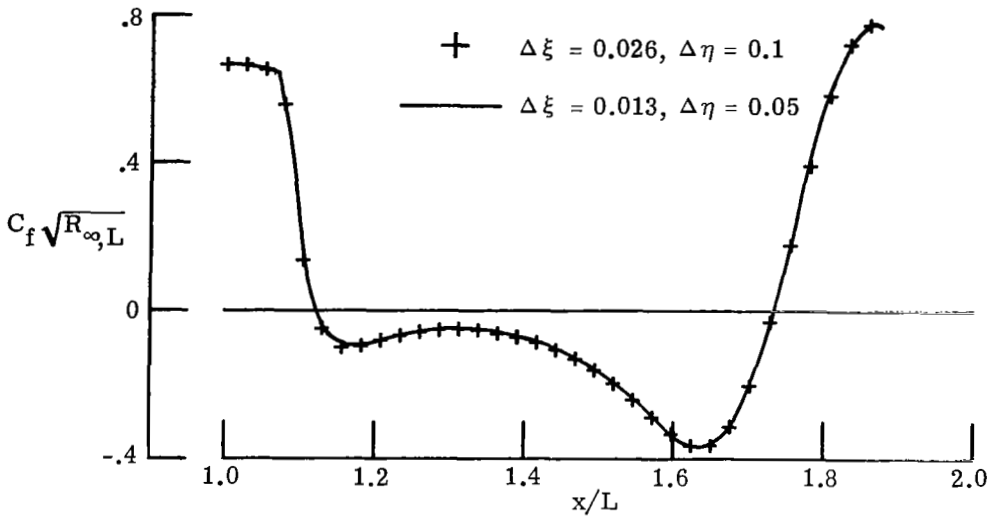

(a) Skin friction.

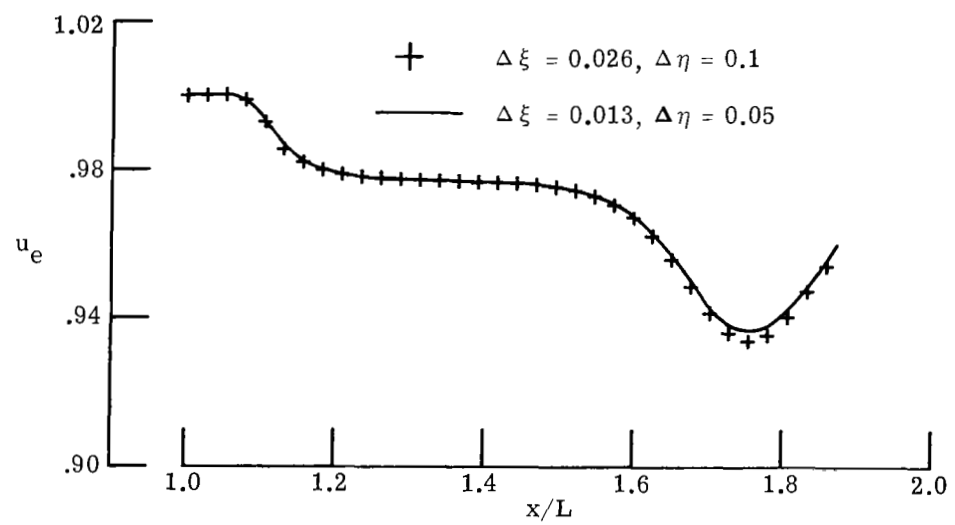

(b) Edge velocity.

Figure 12.- Effect of grid size on calculations for case B.

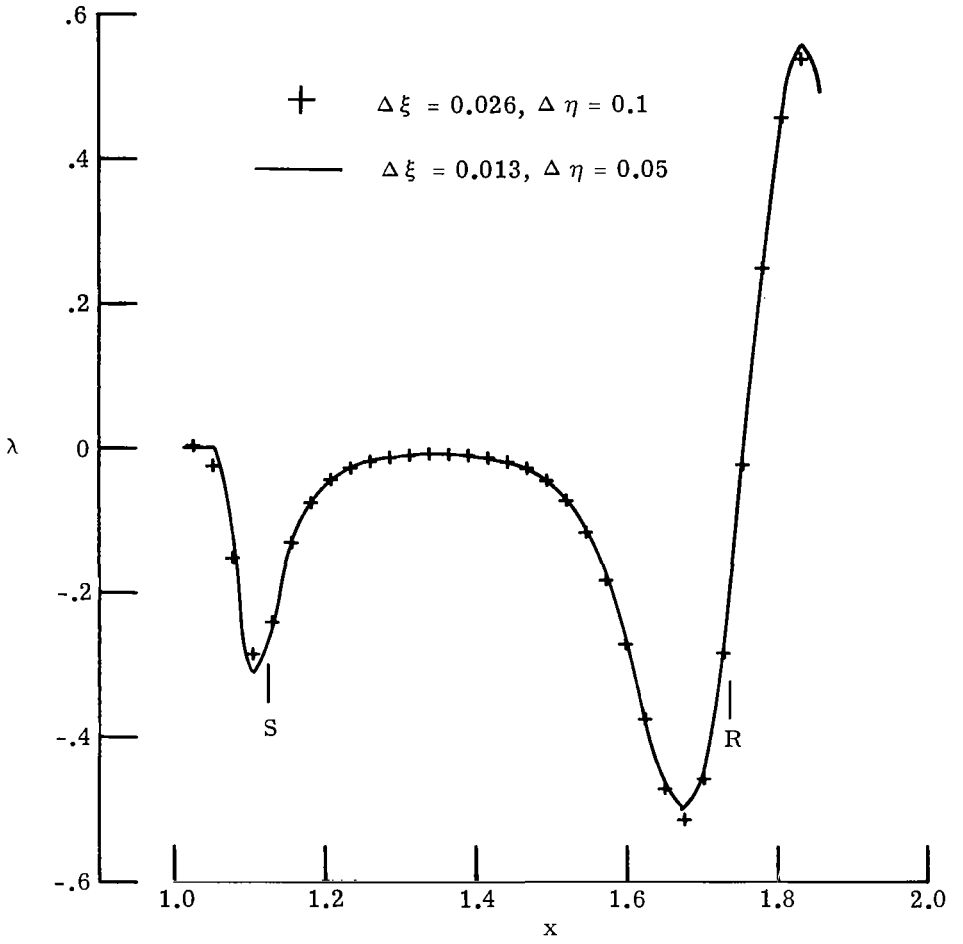

(c) Meksyn pressure-gradient parameter (S = Separation, R = Reattachment).

Figure 12.- Concluded.

Approximate solutions.- All of the calculations discussed herein were recomputed using the approximate forward-marching procedure. In all cases the calculations were stable and, as expected, the agreement between these approximate solutions and the more exact calculations obtained with global iteration becomes poorer as the magnitude of the reverse flow velocity increases. The solutions were almost identical in the Briley and Klineberg and Steger cases. The magnitude of the skin-friction distributions for cases A and B obtained by the forward-marching technique and by the global iterative procedure are shown in figure 13. The agreement is quite good in case A where the maximum reverse flow velocity is $-0.05U_\infty$; in case B where the velocity is about $-0.10U_\infty$, the accuracy of the reversed flow approximation is slightly less. For case B the approximate technique predicts about the same reattachment point as the more accurate global scheme (fig. 13). Therefore, at least for this case, the solution beyond reattachment does not appear to be affected by the local errors made in the reversed flow region.

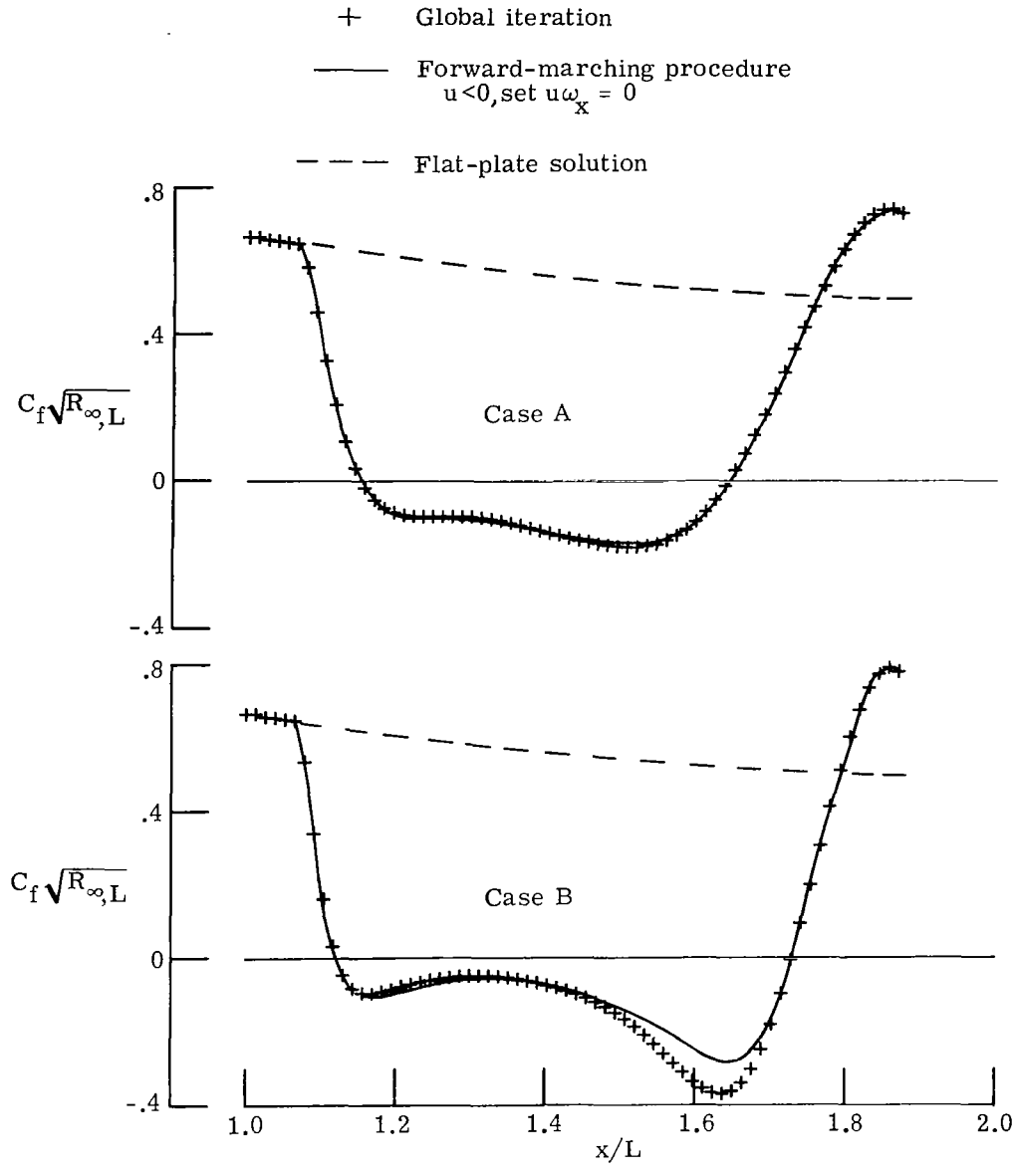

Figure 13.- Comparison of skin friction for global and forward-marching procedure for cases A and B.

Klineberg and Steger also converted their global iterative procedure in which the wall shear is prescribed to a forward-marching technique. They included the Reyhner and Flügge-Lotz approximation and used a backward difference on $\partial u/\partial x$ in the continuity equation. However, their calculations were unstable except when a coarse grid was used with a first-order scheme in the stream direction. The instability occurred even though the magnitude of the reverse flow velocity was less than $0.02U_\infty$. In contrast, in the present calculations, some of which are for more severe separation cases, no instabilities were encountered even with further grid refinements, when the streamwise con-

vection of vorticity in the reversed flow region was neglected. Since both the reversed flow approximations and the problem formulations are different in these two studies, it is difficult to assess precisely why the present results are stable and those of Klineberg and Steger are not.

The reduction in computer storage obtained by using the Reyhner and Flügge-Lotz approximation is substantial since only two columns of data need to be stored. In contrast, an entire plane of data is required in the global procedure. Significant reductions in computer time are also achieved. For example, in the present calculation of Briley's case, the total computer time required in the approximate calculation for 5700 grid points was about 1 minute on the CDC 6600 computer system; 5.5 minutes (131 iterations) were required in the global iterative procedure. Both of these computer times are significantly less than the 45 minutes used by Briley for the Navier-Stokes equations for 1050 grid points on the UNIVAC 1108. The computational speed of the CDC 6600 is approximately four times that of the UNIVAC 1108.

It was found that the convergence of the global procedure could be accelerated considerably by using the approximate solution as initial conditions. Table I shows the number of global iterations required for convergence when crude initial conditions (upstream boundary condition repeated at each streamwise station) are used in comparison with the use of the approximate solution. The average number of column iterations required at each x station in the forward-marching procedure are also shown in table I. As expected, table I shows that this convergence acceleration becomes less as the magnitude of the reverse flow velocity increases and the reversed flow approximation becomes poorer. Use of the crude initial conditions resulted in an unstable calculation in case B; whereas, a converged solution was found by using improved initial conditions.

TABLE I.- EFFECT OF INITIAL CONDITIONS ON TOTAL NUMBER OF GLOBAL ITERATIONS WITH δ^* PRESCRIBED

Case	Number of global iterations		Average number of column iterations forward-marching procedure	Maximum negative, u
	Crude initial conditions	Initial conditions from forward-marching procedure		
Briley	131	26	10	-0.01
Klineberg and Steger ($\hat{\alpha}$ = 0.1)	216	27	13	-.02
A, coarse grid	145	29	18	-.05
A, fine grid	205	114	14	-.05
B, coarse grid	Unstable	130	41	-.10
B, fine grid	Unstable	166	28	-.10

Prescribed Wall Shear

Comparison with solutions of the Navier-Stokes equations.- The wall shear computed by Briley (fig. 4) is used as a prescribed boundary condition for formulation 1. The resulting displacement thickness is shown in figure 14 to be in excellent agreement with that obtained by Briley. Similar agreement of the velocity profiles at various streamwise stations is also found. This prescribed wall-shear calculation for the Briley case required 219 iterations for convergence as compared to 106 and 131 iterations which were required for the coarse and fine grid calculations, respectively, with δ^* prescribed. This result is somewhat surprising as it was originally thought that the solution would converge more rapidly with the wall shear prescribed than with δ^* prescribed, since in the latter formulation the wall vorticity is unknown and must be deduced along with the solution.

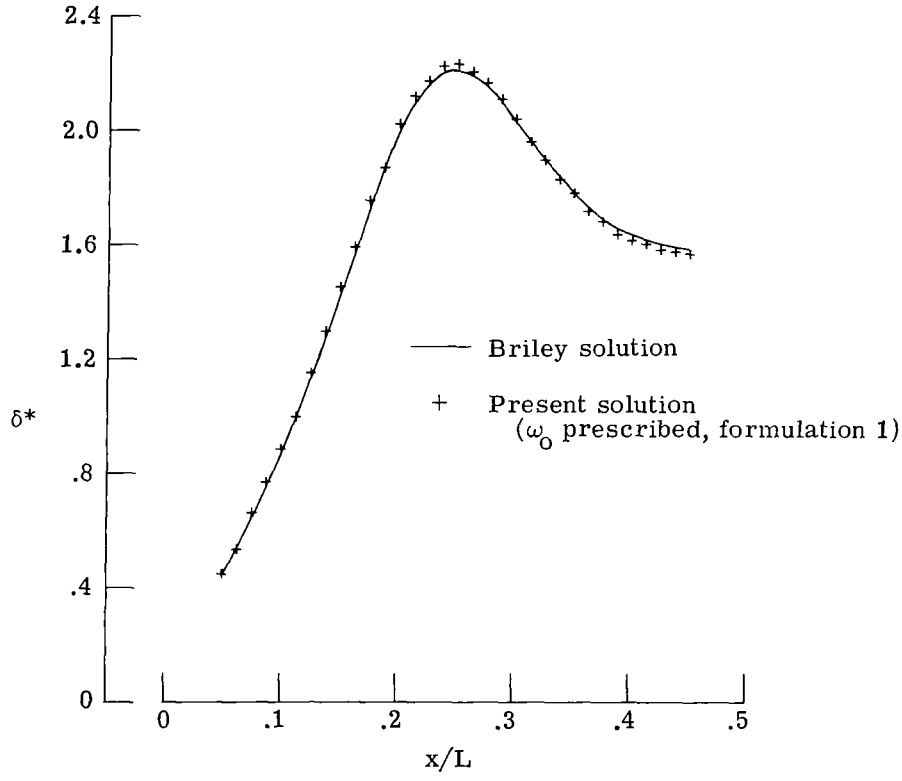

Figure 14.- Comparison of computed displacement thickness distributions.

Discontinuous solutions: formulation 1.- Despite the excellent agreement obtained in the comparison with Briley's calculation, in several additional calculations with formulation 1, solutions were obtained which contain a streamwise discontinuity. For example, the previously discussed Klineberg and Steger case (for $\hat{\alpha} = 0.1$) was calculated with the skin-friction distribution shown in figure 7 as a prescribed condition. In figure 15 the resulting solution for the edge velocity u_e obtained from the velocity profile is compared

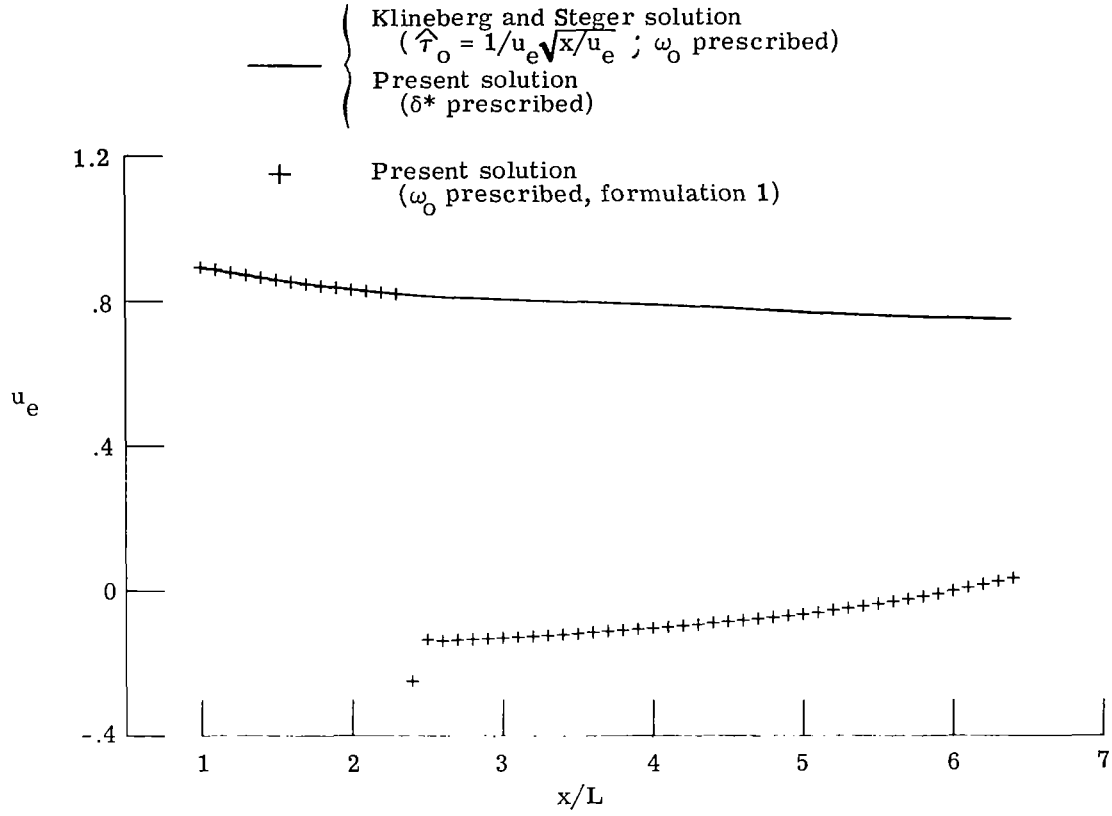

Figure 15.- Discontinuous solution for edge velocity, $\hat{\alpha} = 0.1$.

with that found by Klineberg and Steger; their solution is the same as that deduced in the present formulation with δ^* prescribed. A discontinuity in u_e is observed at $x = 2.4$, a point which is a short distance downstream of the prescribed separation point. The edge velocity u_e is negative between the discontinuity and the prescribed reattachment point $x = 6.0$. In this region the u component of velocity varies monotonically from the wall to the asymptotic edge value shown in figure 15; hence, in this region the entire boundary-layer flow is in the negative x direction. At the x location of the discontinuity, the v component of velocity has a sudden increase followed by a rapid decrease. This large outflow from the boundary layer in the vicinity of the discontinuity is expected, since most of the flow is forward just before the discontinuity and all the flow is reversed just after the discontinuity. It should be noted that this calculation required 609 iterations to converge. The same results were obtained when the calculation was repeated with Δx increased from 0.1 to 0.2.

This calculation converged. However, it is not a valid solution to the boundary-layer equations, since the profile value of u_e (obtained from eq. (50) with $\eta \to \infty$) does not agree with that obtained from evaluating the x momentum equation at the wall (given in

eq. (51)). In formulation 2 these two values of u_e are forced to be equal. Using this formulation, this case was recomputed with the resulting u_e distribution smooth and in excellent agreement with that obtained by Klineberg and Steger. Good agreement is obtained in the resulting δ^* distributions which are shown in figure 16. The present calculation required about 500 iterations to converge. As noted in the Briley case already discussed, this number of iterations is considerably more than the 216 iterations required in the prescribed δ^* calculation. Thus, it is deduced that, in certain calculations, specification of zero vorticity at the boundary-layer edge is not an adequate boundary condition to obtain a valid solution. Rather, it appears necessary to require the unknown velocity at the boundary-layer edge to be the same as that deduced from the pressure gradient in equation (51). In contrast, no discontinuities were encountered in any of the calculations with δ^* prescribed since, in a similar manner, the flow in the boundary layer is controlled by setting the transformed stream function $\tilde{\psi}$ equal to zero at the outer boundary.

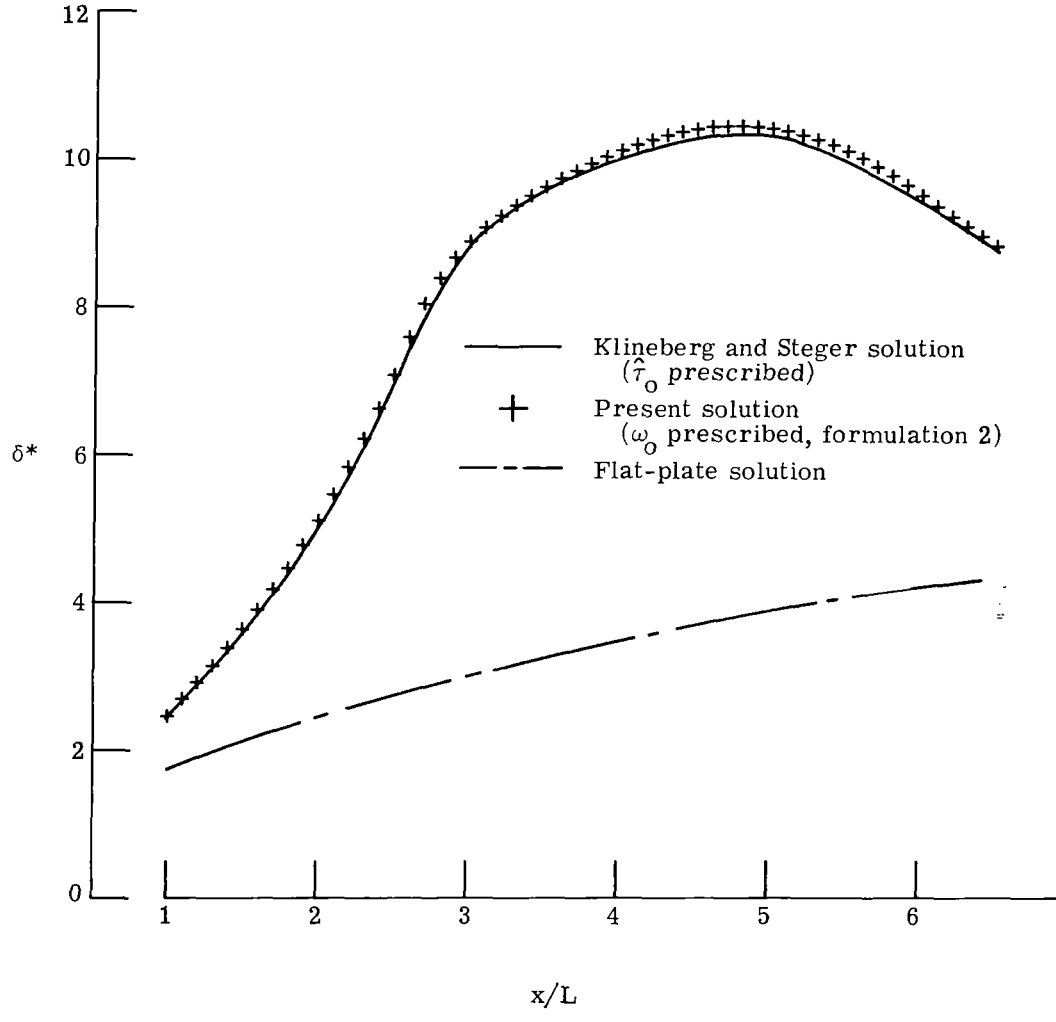

Figure 16.- Comparison of computed displacement thickness distributions, $\hat{\alpha} = 0.1$.

Discontinuous solutions: formulation 3.- Klineberg and Steger encountered an unexplained discontinuity in the pressure-gradient parameter when they set $\hat{\alpha} = 0$ in the prescribed wall shear given in equations (87) and (88). This transformed shear distribution and that distribution for $\hat{\alpha} = 0.1$ used in the calculation discussed above are shown in figure 17. Both of these shear distributions were used as input conditions to the present solution technique using formulation 3. For $\hat{\alpha} = 0.1$, the calculation converged in about 500 iterations and agrees well with the solution obtained by Klineberg and Steger. For $\hat{\alpha} = 0$, a discontinuity occurs in the m distribution which is located at approximately the same x position as that found by Klineberg and Steger (fig. 18). The present numerical technique and problem formulation differ significantly from that of Klineberg and Steger and yet both procedures deduce essentially the same discontinuous solution for $\hat{\alpha} = 0$. Therefore, it is concluded from this calculation that an arbitrarily prescribed wall-shear distribution does not necessarily result in a physically meaningful solution. The cause of this discontinuity is not known. Klineberg and Steger concluded that the discontinuous solution shown in figure 18 may indicate a possible breakdown in the boundary-layer equations. The breakdown may be caused by the relatively large extent of separated flow and the magnitude of the normal component of velocity at the boundary-layer edge. However, this argument is discounted since several cases with smooth solutions involving much larger normal velocities were computed in the present investigations with δ^* prescribed.

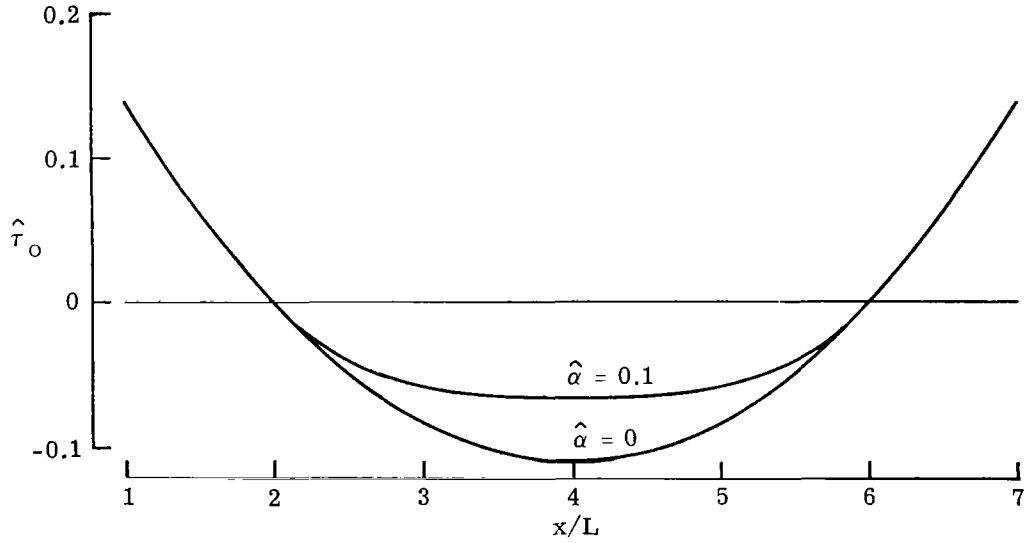

Figure 17.- Prescribed transformed wall-shear distributions.

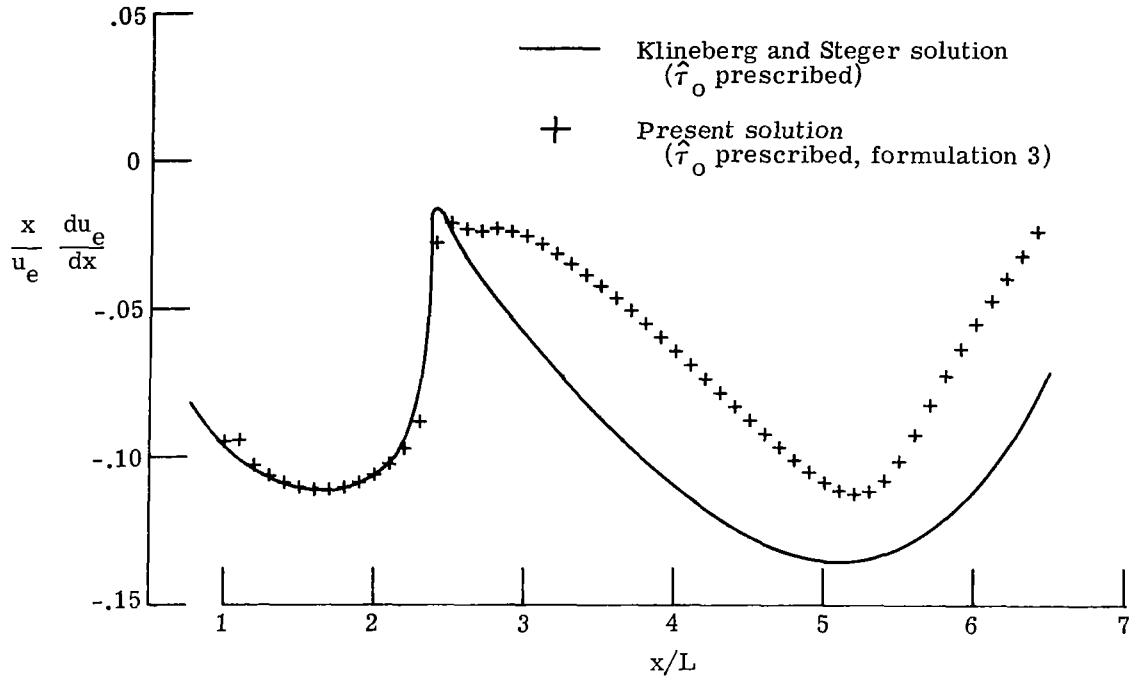

Figure 18.- Discontinuous solution for pressure-gradient parameter, $\hat{\alpha} = 0.1$.

CONCLUDING REMARKS

This report demonstrates that regular solutions of the laminar boundary-layer equations can be obtained at separation with either a prescribed displacement thickness or wall-shear distribution. Excellent agreement was obtained in a comparison of these solution techniques with a calculation of the Navier-Stokes equations made by Briley for a flow having a relatively thin separation bubble terminated by reattachment on a solid surface. Based on this agreement, as well as on that obtained by other investigators for compressible flows, it is concluded that the boundary-layer approximations to the Navier-Stokes equations are adequate for separated laminar flows of limited extent.

The present inverse boundary-layer solutions are obtained by several different global iteration schemes in which the finite-difference scheme is switched in the reversed flow region to account properly for the flow direction. These global schemes have unconditional diagonal dominance and are shown by the von Neumann analysis to have linear stability. As a special case in this analysis, it is concluded that overrelaxation of the diffusion equation results in an unstable calculation, at least with the three finite-difference schemes considered. In the forward flow region, it was essential to use a second-order accurate technique; in the cases considered in this report, first-order accuracy was found adequate in the reversed flow region.

The prescribed displacement thickness method described herein is preferred to the three schemes presented for a prescribed wall shear. For the same case, the results obtained with the wall shear prescribed required approximately twice the number of iterations and twice the computer time as that required with the displacement thickness prescribed. Furthermore, in the wall-shear prescribed formulation, it was necessary to constrain the unknown edge velocity so as to match that velocity deduced from the unknown pressure gradient. Even with this constraint, a discontinuous solution was obtained with the present formulation. The discontinuous solution was found to be similar to that obtained by Klineberg and Steger for the same case. Since the formulations and numerical techniques differ significantly for these two wall-shear prescribed procedures, it is concluded that an arbitrarily prescribed wall shear distribution does not necessarily result in a physically meaningful solution in separated flow. Further research is needed to determine the cause of this streamwise discontinuous behavior which occurs just downstream of the separation point.

An approximate forward-marching procedure is presented. In this procedure, a separated boundary-layer flow is computed in one sweep from the upstream boundary, that is, in the same manner as an attached flow. In the reversed flow region, the streamwise convection of vorticity is set equal to zero to prevent the instability which occurs in marching against the flow. This approximation is similar to that, first introduced by Reyhner and Flügge-Lotz for reversed flow, of neglecting the streamwise convection of momentum. In this approximate scheme, the usual column iterative procedure was modified to give unconditional diagonal dominance. The resulting column iterative scheme is analyzed for linear stability by the von Neumann analysis. This procedure eliminates the need for artificial convection terms which Reyhner and Flügge-Lotz and Werle, Polak, and Bertke added to obtain convergence in their column iterative procedure at each streamwise station.

Comparisons between results obtained with the global iterative procedure and the forward-marching procedure show that the latter is accurate provided the magnitude of the reverse flow velocity is less than about $0.10U_\infty$. The local errors made in the reversed flow region with this approximate scheme are not observed to affect the flow downstream of reattachment, at least for the cases considered. As expected, the number of iterations required for convergence in the global procedure is reduced substantially by using the approximate solution as initial conditions.

Langley Research Center
National Aeronautics and Space Administration
Hampton, Va. 23665
September 5, 1975

APPENDIX A

STABILITY ANALYSIS OF PRESCRIBED DISPLACEMENT THICKNESS METHOD

Attached Flow

The von Neumann stability analysis is applied to the global iterative scheme in equation (37) for the prescribed displacement thickness method for both attached and separated flows. Attached flow is considered first. Substituting for A_n, B_n, C_n, and D_n from equation (18) into equation (37) gives

$$
\begin{aligned}
&-\frac{1}{2}\left(C_\eta + 1\right)\omega^{j+1}_{m,n-1} + \left(2C_\xi + 1 + \alpha\right)\omega^{j+1}_{m,n} + \frac{1}{2}\left(C_\eta - 1\right)\omega^{j+1}_{m,n+1} \\
&= \alpha\omega^{j}_{m,n} + r\left[\frac{1}{2}\left(C_\eta + 1\right)\omega^{j+1}_{m-1,n-1} + \left(2C_\xi - 1\right)\omega^{j+1}_{m-1,n} - \frac{1}{2}\left(C_\eta - 1\right)\omega^{j+1}_{m-1,n+1}\right] \\
&+ (1 - r)\left[-\frac{1}{2}\left(C_\eta + 1\right)\omega^{j}_{m,n-1} + \left(2C_\xi + 1\right)\omega^{j}_{m,n} + \frac{1}{2}\left(C_\eta - 1\right)\omega^{j}_{m,n+1}\right]
\end{aligned}
\tag{A1}
$$

where the coefficients C_ξ, C_η, and α, which are held constant in the von Neumann analysis, are evaluated with the most recent solution. A Fourier component of arbitrary wave numbers, k_ξ and k_η, is written as

$$
\omega^{j}_{m,n} = \Omega^{j}_{o} \exp i\left(k_\xi \xi + k_\eta \eta\right) \tag{A2}
$$

where Ω^{j}_{o} is the amplitude coefficient at the jth iteration. Substitution of equation (A2) into equation (A1) gives the amplification factor $|g| = |N|/|D|$ where

$$
\left.
\begin{aligned}
N &= \alpha + (1 - r)\left(1 - \cos\phi + 2C_\xi\right) + i(1 - r)C_\eta \sin\phi \\
D &= \alpha + (1 + r\cos\theta)(1 - \cos\phi) + 2C_\xi(1 - r\cos\theta) + rC_\eta \sin\theta \sin\phi \\
&\quad + i\left[r\sin\theta\left(2C_\xi - 1 + \cos\phi\right) + C_\eta \sin\phi(1 + r\cos\theta)\right]
\end{aligned}
\right\} \tag{A3}
$$

where $\theta = k_\xi \Delta\xi$ and $\phi = k_\eta \Delta\eta$. Note that the range of ϕ and θ values is $0 \leqq (\phi, \theta) \leqq \pi$ and corresponds to the range of solution wavelengths $\left(\ell_\xi \text{ and } \ell_\eta\right)$ of

$$\left.\begin{aligned} \infty \geqq l_\xi \geqq 2\ \Delta\xi \\ \infty \geqq l_\eta \geqq 2\ \Delta\eta \end{aligned}\right\} \tag{A4}$$

since k_ξ and k_η can be expressed as

$$\left.\begin{aligned} k_\xi = \frac{2\pi}{l_\xi} \\ k_\eta = \frac{2\pi}{l_\eta} \end{aligned}\right\} \tag{A5}$$

The requirement for stability is that $|g| \leqq 1$. It is convenient to consider the stability requirement in the form $|g|^2 \leqq 1$ which becomes

$$D^2 - N^2 \geqq 0 \tag{A6}$$

Expressing equation (A3) in the form of equation (A6) results in

$$r\left\{(1 + \cos\theta)(1 - \cos\phi)(\alpha + 1 - \cos\phi) + \left(C_\eta \sin\phi\sqrt{1 + \cos\theta} + 2C_\xi\sqrt{1 - \cos\theta}\right)^2\right.$$
$$\left. + 2C_\xi\left[\alpha(1 - \cos\theta) + 2(1 - r)(1 - \cos\phi)\right] + C_\eta\alpha \sin\theta \sin\phi\right\} \geqq 0 \tag{A7}$$

Equation (A7) must be satisfied to prevent instability.

Equation (A7) is first considered in the limit of $\Delta\xi$ and $\Delta\eta \to 0$ with $C_\xi = \frac{u\delta^{*2}\ \Delta\eta^2}{2\ \Delta\xi}$ held constant so as to preserve the highest ξ and η derivatives. Since $\alpha \sim C_\eta \sim \Delta\eta$ then with α and C_η set equal to zero, equation (A7) reduces

$$(1 + \cos\theta)(1 - \cos\phi)^2 + 4C_\xi{}^2(1 - \cos\theta) + 4C_\xi(1 - r)(1 - \cos\phi) \geqq 0 \tag{A8}$$

Equation (A8) must be satisfied for stability in the relaxation solution of the diffusion equation

$$u\delta^{*2}\frac{\partial\omega}{\partial\xi} = \frac{\partial^2\omega}{\partial\eta^2} \tag{A9}$$

with the Crank-Nicholson scheme. Equation (A8) is rearranged to give

$$r \leqq 1 + \frac{(1 + \cos\theta)(1 - \cos\phi)}{4C_\xi} + \frac{(1 - \cos\theta)C_\xi}{1 - \cos\phi} \tag{A10}$$

The maximum value allowed for the relaxation factor is found by letting $C_\xi \sim \phi \sim \theta \to 0$ which results in

$$r \leqq 1 + \frac{5\phi}{4} + \ldots \tag{A11}$$

and hence $r \leqq 1$ for stability. Thus, overrelaxation cannot be used in obtaining a relaxation solution of the diffusion equation with the Crank-Nicholson scheme.

Equation (A7) is now examined to see if the lower order terms may result in the violation of this inequality. With $r \leqq 1$, and since C_ξ and α are positive, then all of the terms in equation (A7) are positive with the exception of the last which is negative when $C_\eta < 0$. The largest negative value of C_η occurs as the boundary-layer edge is approached. In such a case,

$$C_\eta \approx -\frac{\Delta\eta}{2} u_e \delta^*(\eta - 1)\frac{d\delta^*}{d\xi} \tag{A12}$$

where $C_\eta < 0$ if $d\delta^*/d\xi > 0$. Therefore, as the positive slope of the prescribed displacement thickness increases, the destabilizing influence of the lower order term is increased. Obviously the effect of this term can be reduced by decreasing $\Delta\eta$. In practice, the calculations were performed without regard to this observation; hence, the only stability restriction is $r \leqq 1$ which is deduced from the consideration of the higher order terms. This condition is consistent with the observation of Richtmyer and Morton that the stability of many finite-difference solutions of the diffusion equation is essentially unaffected by the presence of lower order terms.

The only evidence of instability caused by the lower order terms occurred in the calculation in which the prescribed displacement thickness is case B shown in figure 9. This case is the most severe separation calculation considered in this report. In this case, very small amplitude oscillations occur in the η distribution of vorticity near the boundary-layer edge. In this region the negative values of C_η are sufficiently large to cause $|g|$ to exceed slightly unity for certain values of ϕ and θ. The stability of the calculation is presumed to be enhanced by the imposition of the outer boundary conditions; of course, these conditions are not accounted for in the von Neumann analysis. It was observed that the magnitude of these oscillations was reduced by decreasing $\Delta\eta$ as

anticipated from equation (A7). Furthermore, the oscillations were entirely eliminated by using a first-order scheme in which a von Neumann analysis shows that the lower order terms do not have any destabilizing effect.

The same calculation discussed in the preceding paragraph was used to test several values of the relaxation factor. With reasonably accurate initial conditions provided by an approximate forward-marching procedure, calculations were made for the different values of the relaxation factor of 0.4, 7, 1.0, 1.1, and 1.5. Only in the case of $r = 0.4$ was convergence observed. However, the behavior of the maximum residual (increment in vorticity between two successive iterations) is distinctly different depending on whether $r \leqq 1$ or $r > 1$. In both cases the maximum vorticity residual occurs at the surface. However, for $0.4 < r \leqq 1.0$ this residual, although small, has an oscillatory behavior and convergence is never obtained. In contrast, for $r > 1.0$ the solution diverges rapidly in a manner which suggests that the von Neumann stability criterion has been violated. It is concluded from these calculations that whereas the von Neumann analysis requires $r \leqq 1$ as a necessary condition for stability, the actual value of r may need to be less than unity because of the calculation of the surface vorticity.

Alternate Scheme for Attached Flow

For $r = 1$, equation (A1) can be interpreted as the finite-difference representation of the unsteady vorticity-transport equation

$$\frac{\partial \omega}{\partial t} + a \frac{\partial \omega}{\partial \xi} + b \frac{\partial \omega}{\partial \eta} = \frac{\partial^2 \omega}{\partial \eta^2} \tag{A13}$$

where the time derivative is

$$\frac{\partial \omega}{\partial t} = \frac{\omega_{m,n}^{j+1} - \omega_{m,n}^{j}}{\Delta t} \tag{A14}$$

with $\Delta t = \Delta \eta^2 / \alpha$ and where a and b represent the coefficients in equation (12). In an attempt to eliminate the destabilizing effect of the lower order terms found in the previous scheme the time derivative, which is introduced to establish diagonal dominance, is given by

$$\frac{\partial \omega}{\partial t} = \frac{1}{2}\left(\frac{\omega_{m,n}^{j+1} - \omega_{m,n}^{j}}{\Delta t} + \frac{\omega_{m-1,n}^{j+1} - \omega_{m-1,n}^{j}}{\Delta t} \right) \tag{A15}$$

A comparison of the computational molecules of these two schemes in figure 19 shows the symmetry of the alternate scheme. This alternate global scheme can be written as follows by using equation (A15) with $\alpha = \Delta \eta^2 / 2\,\Delta t$ and after introducing a relaxation factor as was done previously:

APPENDIX A

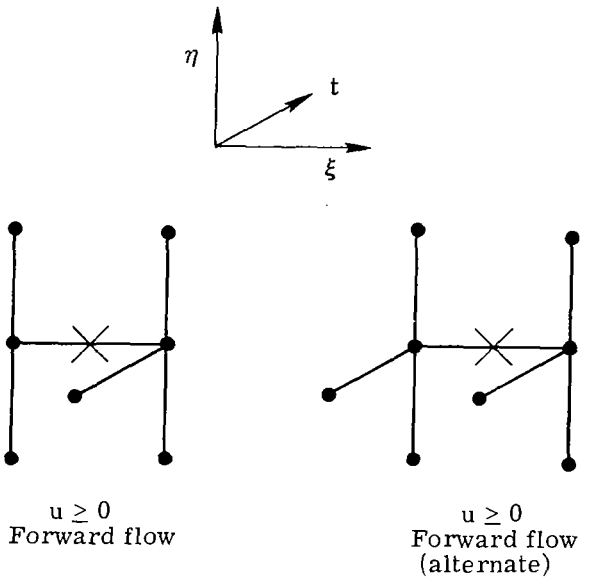

Figure 19.- Time-like interpretation of iterative finite-difference schemes.

$$-\frac{1}{2}\left(C_\eta + 1\right)\omega^{j+1}_{m,n-1} + \left(2C_\xi + 1 + \alpha\right)\omega^{j+1}_{m,n} + \frac{1}{2}\left(C_\eta - 1\right)\omega^{j+1}_{m,n+1}$$

$$= \alpha\omega^{j}_{m,n} + r\alpha\omega^{j}_{m-1,n} + r\left[\frac{1}{2}\left(C_\eta + 1\right)\omega^{j+1}_{m-1,n-1} + \left(2C_\xi - 1 - \alpha\right)\omega^{j+1}_{m-1,n} - \frac{1}{2}\left(C_\eta - 1\right)\omega^{j+1}_{m-1,n+1}\right]$$

$$+ (1 - r)\left[-\frac{1}{2}\left(C_\eta + 1\right)\omega^{j}_{m,n-1} + \left(2C_\xi + 1\right)\omega^{j}_{m,n} + \frac{1}{2}\left(C_\eta - 1\right)\omega^{j}_{m,n+1}\right] \tag{A16}$$

The amplification factor for this scheme is $|g| = |N|/|D|$ where

$$\left.\begin{aligned} N &= \alpha(1 + r\cos\theta) + (1 - r)\left(2C_\xi + 1 - \cos\phi\right) + i\left[-\alpha r\sin\theta + (1 - r)C_\eta\sin\phi\right] \\ D &= \alpha(1 + r\cos\theta) + (1 + r\cos\theta)(1 - \cos\phi) + 2C_\xi(1 - r\cos\theta) + rC_\eta\sin\phi\sin\theta \\ &\quad + i\left[r\sin\theta\left(2C_\xi - 1 + \cos\phi - \alpha\right) + C_\eta\sin\phi(1 + r\cos\theta)\right] \end{aligned}\right\} \tag{A17}$$

The requirement for stability $|g|^2 \leqq 1$ becomes

APPENDIX A

$$D^2 - N^2 = r\left\{(1 + \cos\theta)(1 - \cos\phi)\left[(1 + r)\alpha + 1 - \cos\phi\right] + \left(C_\eta \sin\phi\sqrt{1 + \cos\theta} + 2C_\xi\sqrt{1 - \cos\theta}\right)^2 + 2(1 - r)C_\xi\left[(1 - \cos\theta)\alpha + 2(1 - \cos\phi)\right] + (1 - r)C_\eta\alpha \sin\theta \sin\phi\right\} \geqq 0 \tag{A18}$$

In the limit of zero mesh size with $\Delta\eta^2/\Delta\xi$ held constant, this scheme reduces to the same as that previously considered and, hence, $r \leqq 1$ is required for stability. With $r \leqq 1$ all of the terms in equation (A18) are positive except for the last which is negative if $r \neq 1$ and $C_\eta < 0$. Thus, in this global iterative scheme the possible destabilizing influence of the lower order term is eliminated provided no underrelaxation is used. Unfortunately, the advantage of this scheme could not be used in the present study since a smaller value of the relaxation factor was found to be necessary in the calculations, primarily because of the computation of the surface vorticity.

Separated Flow

The stability analysis of the global iterative scheme for separated flow proceeds in an analogous manner to that for attached flow. Substituting for A_n, B_n, C_n, and D_n from equation (21) into equation (37) gives

$$-\left(C_\eta + 1\right)\omega^{j+1}_{m,n-1} + \left(\alpha + 2 - 2C_\xi\right)\omega^{j+1}_{m,n} + \left(C_\eta - 1\right)\omega^{j+1}_{m,n+1}$$

$$= \alpha\omega^{j}_{m,n} + (1 - r)\left[-\left(C_\eta + 1\right)\omega^{j}_{m,n-1} + 2\left(1 - C_\xi\right)\omega^{j}_{m,n} + \left(C_\eta - 1\right)\omega^{j}_{m,n+1}\right] - 2rC_\xi\omega^{j}_{m+1,n} \tag{A19}$$

Since $C_\xi < 0$ for separated flow, it is convenient to set $C_\xi = -\left|C_\xi\right|$. The substitution of equation (A2) into equation (A19) gives the amplification factor

$$\left|g\right| = \frac{\left|\Omega^{j+1}_o\right|}{\left|\Omega^{j}_o\right|}$$

$$= \frac{\left|\frac{\alpha}{2} + \left[1 - r(1 - \cos\theta)\right]\left|C_\xi\right| + (1 - r)(1 - \cos\phi) + i\left[(1 - r)C_\eta \sin\phi + r\left|C_\xi\right| \sin\theta\right]\right|}{\left|\frac{\alpha}{2} + \left|C_\xi\right| + 1 - \cos\phi + iC_\eta \sin\phi\right|} \tag{A20}$$

APPENDIX A

Expressing equation (A20) in the form of equation (A6) results in

$$r\left\{(1 - r)(1 - \cos\theta)\left|C_\xi\right|^2 - (1 - r)\sin\phi\sin\theta\left|C_\xi\right|C_\eta + \left(\frac{2 - r}{2}\right)\sin^2\phi\, C_\eta{}^2 + \left(\frac{2 - r}{2}\right)\right.$$

$$\left.\times (1 - \cos\phi)^2 + \frac{\alpha}{2}\left[(1 - \cos\phi) + \left|C_\xi\right|(1 - \cos\theta)\right] + \left|C_\xi\right|(1 - \cos\phi)\left[2 - r - (1 - r\cos\theta)\right]\right\} \geqq 0 \tag{A21}$$

which must be satisfied to prevent instability. First the limit of zero mesh size is considered, which again implies the solution of the diffusion equation by relaxation. Setting $\Delta\eta$ and $\Delta\xi$ equal to zero with C_ξ held constant results in

$$(1 - r)(1 - \cos\theta)\left|C_\xi\right|^2 + \left(\frac{2 - r}{2}\right)(1 - \cos\phi)^2 + \left|C_\xi\right|(1 - \cos\phi)\left[2 - r - (1 - r\cos\theta)\right] \geqq 0 \tag{A22}$$

Equation (A22) is satisfied if $r \leqq 1$. With this restriction on the relaxation factor, all of the terms in equation (A21) are positive with the exception of the second term which is negative when $C_\eta > 0$. However, it is shown here that the first three terms of equation (21) are always positive; hence, if $r \leqq 1$, then equation (A21) is always satisfied. The first three terms of equation (A21) can be rewritten as

$$\left[\sqrt{(1 - r)(1 - \cos\theta)}\left|C_\xi\right| - \sqrt{\frac{2 - r}{2}}\sin\phi C_\eta\right]^2 + \left\{2\left[(1 - r)\left(\frac{2 - r}{2}\right)(1 - \cos\theta)\right]^{1/2}\right.$$

$$\left. - (1 - r)\sin\theta\sin\phi\left|C_\xi\right|C_\eta\right\} \tag{A23}$$

With $r \leqq 1$ and $C_\eta > 0$ (worst case), the quantity in braces in equation (A23) is positive and the von Neumann condition is satisfied. Thus, the first-order global iteration scheme used for separated flow is stable provided that overrelaxation, that is, when $r > 1$, is not used.

APPENDIX B

STABILITY ANALYSIS OF PRESCRIBED WALL-SHEAR METHOD

The von Neumann stability analysis is applied in this appendix to the global iterative scheme used for the vorticity transport equation in the prescribed wall-shear method. Only attached flow is considered since the reversed flow scheme is the same as that used in the prescribed displacement thickness method. Substituting for A_n, B_n, C_n, and D_n from equation (75) into equation (37) gives

$$-\left(C_\eta + 1\right)\omega^{j+1}_{m,n-1} + \left(2 + 3C_\xi + \alpha\right)\omega^{j+1}_{m,n} + \left(C_\eta - 1\right)\omega^{j+1}_{m,n+1}$$

$$= \alpha\omega^{j}_{m,n} + (1 - r)\left[-\left(C_\eta + 1\right)\omega^{j}_{m,n-1} + \left(2 + 3C_\xi\right)\omega^{j}_{m,n} + \left(C_\eta - 1\right)\omega^{j}_{m,n+1}\right]$$

$$+ rC_\xi\left(4\omega^{j+1}_{m-1,n} - \omega^{j+1}_{m-2,n}\right) \tag{B1}$$

where the coefficients C_ξ, C_η, and α are given in equations (75) and (76). The substitution of equation (A2) into equation (B1) gives the amplification factor

$$|g| = \frac{\left|\alpha + 2(1 - r)(1 - \cos\phi) + 3(1 - r)C_\xi + i\left[2(1 - r)C_\eta \sin\phi\right]\right|}{\left|\alpha + 2(1 - \cos\phi) + C_\xi\left[3 - r(4\cos\theta - \cos 2\theta)\right] + i\left[2C_\eta \sin\phi + rC_\xi(4\sin\theta - \sin 2\theta)\right]\right|} \tag{B2}$$

In the case of no underrelaxation, that is, when $r = 1$, equation (B2) becomes

$$|g| = \frac{|\alpha|}{\left|\alpha + 2(1 - \cos\phi) + 2C_\xi(1 - \cos\theta)^2 + i\left[2C_\eta \sin\phi + C_\xi(4\sin\theta - \sin 2\theta)\right]\right|} \tag{B3}$$

which satisfies the von Neumann condition $|g| \leqq 1$ since $C_\xi \geqq 0$ and $\alpha \geqq 0$.

For a more general value of r it is convenient to rewrite the von Neumann condition $|g| = |N|/|D|$ as

$$D^2 - N^2 \geqq 0 \tag{B4}$$

Expressing equation (B2) in the form of equation (B4) gives

$$r\Big\{\Big[3 - 3\cos\theta(2 - \cos\theta) + 2r(1 - \cos\theta)\Big]C_\xi{}^2 + 2\sin\theta\sin\phi(2 - \cos\theta)C_\xi C_\eta$$

$$+ (2 - r)\sin^2\phi C_\eta{}^2 + (1 - \cos\phi)\Big[3(2 - r) - 4\cos\theta + \cos 2\theta\Big]C_\xi$$

$$+ \alpha\Big[(1 - \cos\theta)^2 C_\xi + (1 - \cos\phi)\Big] + (2 - r)(1 - \cos\phi)^2\Big\} \geqq 0 \tag{B5}$$

In the limit of $\Delta\xi$ and $\Delta\eta$ equal to zero with C_ξ held constant, equation (B5) reduces to

$$r\Big\{\Big[3 - 3\cos\theta(2 - \cos\theta) + 2r(1 - \cos\theta)\Big]C_\xi{}^2 + (1 - \cos\phi)\Big[3(2 - r) - 4\cos\theta + \cos 2\theta\Big]C_\xi$$

$$+ (2 - r)(1 - \cos\phi)^2\Big\} \geqq 0 \tag{B6}$$

The most restrictive condition on r is deduced from equation (B6) in the limiting case of $C_\xi \sim \theta \sim \phi \to 0$ which results in $r \leqq 1$. This result is the same as that found previously in this report for several other relaxation schemes for the diffusion equation.

Examination of equation (B5) with $r < 1$ shows that all of the terms are positive with the exception of the second term which is negative when $C_\eta < 0$. Numerical evaluation of equation (B5) for $C_\eta < 0$ and various values of the remaining parameters showed that this term can be sufficiently large to violate this inequality for $r < 1$. However, this destabilizing term is a lower order term and, hence, its magnitude can be reduced by decreasing $\Delta\eta$. In practice, no instabilities caused by this lower order term were encountered in the calculations.

REFERENCES

1. Klineberg, John M.; and Lees, Lester: Theory of Laminar Viscous-Inviscid Interactions in Supersonic Flow. AIAA J., vol. 7, no. 12, Dec. 1969, pp. 2211-2221.

2. Dwoyer, D. L.: Supersonic and Hypersonic Two-Dimensional Laminar Flow Over a Compression Corner. AIAA Computational Fluid Dynamics Conference, July 1973, pp. 69-83.

3. Werle, M. J.; and Vatsa, V. N.: New Method for Supersonic Boundary-Layer Separations. AIAA J., vol. 12, no. 11, Nov. 1974, pp. 1491-1497.

4. Carter, James E.: Numerical Solutions of the Navier-Stokes Equations for the Supersonic Laminar Flow Over a Two-Dimensional Compression Corner. NASA TR R-385, 1972.

5. Ghia, U.; and Davis, R. T.: Study of Flow Past Blunted Thick Plates With Separation and Shoulder Singularity Using Navier-Stokes Equations. AIAA Paper No. 74-12, Jan.-Feb. 1974.

6. Brown, S. N.; and Stewartson, K.: Laminar Separation. Annual Review of Fluid Mechanics, William R. Sears and Milton Van Dyke, eds., Volume 1, Annual Reviews, Inc., 1969, pp. 45-72.

7. Terrill, R. M.: Laminar Boundary-Layer Flow Near Separation With and Without Suction. Phil. Trans. Royal Soc., (London), Ser. A, vol. 253, no. 1022, Sept. 8, 1960, pp. 55-100.

8. Werle, M. J.; and Davis, R. T.: Incompressible Laminar Boundary Layers on a Parabola at Angle of Attack. A Study of the Separation Point. Trans. ASME: J. Appl. Mech., ser. E, vol. 39, no. 1, Mar. 1972, pp. 7-12.

9. Klineberg, John M.; and Steger, Joseph L.: On Laminar Boundary-Layer Separation. AIAA Paper No. 74-94, Jan.-Feb. 1974.

10. Goldstein, S.: On Laminar Boundary-Layer Flow Near a Position of Separation. Quart. J. Mech. & Appl. Math., vol. I, 1948, pp. 43-69.

11. Catherall, D.; and Mangler, K. W.: The Integration of the Two-Dimensional Laminar Boundary-Layer Equations Past the Point of Vanishing Skin Friction. J. Fluid Mech., vol. 26, pt. 1, Sept. 1966, pp. 163-182.

12. Kuhn, Gary D.; and Nielsen, Jack N.: Prediction of Turbulent Separated Boundary Layers. AIAA Paper No. 73-663, July 1973.

13. Horton, Harry P.: Separating Laminar Boundary Layers With Prescribed Wall Shear. AIAA J., vol. 12, no. 12, Dec. 1974, pp. 1772-1774.

14. Klineberg, John M.; and Steger, Joseph L.: Calculation of Separated Flows at Subsonic and Transonic Speeds. Proceedings of the Third International Conference on Numerical Methods in Fluid Mechanics, Volume II. Volume 19 of Lecture Notes in Physics, Henri Cabannes and Roger Temam, eds., Springer-Verlag, 1973, pp. 161-168.

15. Tai, Tsze C.: Transonic Laminar Viscous-Inviscid Interaction Over Airfoils. AIAA Paper No. 74-600, June 1974.

16. Keller, Herbert B.; and Cebeci, Tuncer: An Inverse Problem in Boundary-Layer Flows: Numerical Determination of Pressure Gradient in a Given Wall Shear. J. Comput. Phys., vol. 10, no. 1, Aug. 1972, pp. 151-161.

17. Cebeci, T.; and Witherspoon, G. F.: Theoretical Suction and Pressure Distribution Bounds for Flow Separation in Retarded Flow. J. Aircraft, vol. 11, no. 1, Jan. 1974, pp. 61-64.

18. Briley, W. R.; and McDonald, H.: Numerical Prediction of Incompressible Separation Bubbles. J. Fluid Mech., vol. 69, pt. 4, June 1975, pp. 631-656.

19. Carter, James E.: Solutions for Laminar Boundary Layers With Separation and Reattachment. AIAA Paper No. 74-583, June 1974.

20. Carter, James E.; and Wornom, Stephen F.: A Forward Marching Procedure for Separated Boundary-Layer Flows. AIAA J., vol. 13, no. 8, Aug. 1975, pp. 1101-1103.

21. Carter, James E.; and Wornom, Stephen F.: Solutions for Incompressible Separated Boundary Layers Including Viscous-Inviscid Interaction. Aerodynamic Analyses Requiring Advanced Computers, Part I, NASA SP-347, 1975, pp. 125-150.

22. Reyhner, T. A.; and Flügge-Lotz, I.: The Interaction of a Shock Wave With a Laminar Boundary Layer. Int. J. Non-Linear Mech., vol. 3, no. 2, June 1968, pp. 173-199.

23. Werle, M. J.; Polak, A.; and Bertke, S. D.: Supersonic Boundary-Layer Separation and Reattachment – Finite Difference Solutions. Rep. No. AFL 72-12-1, Naval Air Systems Command, Jan. 1973. (Available from DDC as AD 757 062.)

24. Williams, P. G.: A Reverse Flow Computation in the Theory of Self-Induced Separation. Proceedings of the Fourth International Conference on Numerical Methods in Fluid Dynamics. Volume 35 of Lecture Notes in Physics, Richard D. Richtmyer, ed., Springer-Verlag, 1975, pp. 445-451.

25. Schlichting, Hermann (J. Kestin, transl.): Boundary Layer Theory. Fourth ed. McGraw-Hill Book Co., Inc., c.1960.

26. Ames, William F.: Numerical Methods for Partial Differential Equations. Barres & Noble, Inc., c.1969.

27. Keller, Herbert B.: Numerical Methods for Two-Point Boundary-Value Problems. Blaisdell Pub. Co., c.1968.

28. Richtmyer, Robert D.; and Morton, K. W.: Difference Methods for Initial-Value Problems. Second ed., Interscience Publ., c.1967.

29. Briley, W. Roger: A Numerical Study of Laminar Separation Bubbles Using the Navier-Stokes Equations. J. Fluid Mech., vol. 47, pt. 4, June 1971, pp. 713-736.

30. Howarth, L.: On the Solution of the Laminar Boundary Layer Equations. Proc. Roy. Soc. (London), ser. A, vol. 164, no. 919, Feb. 18, 1938, pp. 547-579.

31. Meksyn, D.: New Methods in Laminar Boundary-Layer Theory. Pergamon Press, Inc., 1961.

32. Schubauer, G. B.: Air Flow in a Separating Laminar Boundary Layer. NACA Rep. 527, 1935.

NATIONAL AERONAUTICS AND SPACE ADMINISTRATION
WASHINGTON, D.C. 20546

OFFICIAL BUSINESS
PENALTY FOR PRIVATE USE $300

SPECIAL FOURTH-CLASS RATE
BOOK

POSTAGE AND FEES PAID
NATIONAL AERONAUTICS AND
SPACE ADMINISTRATION
451

U.S.MAIL

"The aeronautical and space activities of the United States shall be conducted so as to contribute . . . to the expansion of human knowledge of phenomena in the atmosphere and space. The Administration shall provide for the widest practicable and appropriate dissemination of information concerning its activities and the results thereof."

—NATIONAL AERONAUTICS AND SPACE ACT OF 1958

NASA SCIENTIFIC AND TECHNICAL PUBLICATIONS

TECHNICAL REPORTS: Scientific and technical information considered important, complete, and a lasting contribution to existing knowledge.

TECHNICAL NOTES: Information less broad in scope but nevertheless of importance as a contribution to existing knowledge.

TECHNICAL MEMORANDUMS: Information receiving limited distribution because of preliminary data, security classification, or other reasons. Also includes conference proceedings with either limited or unlimited distribution.

CONTRACTOR REPORTS: Scientific and technical information generated under a NASA contract or grant and considered an important contribution to existing knowledge.

TECHNICAL TRANSLATIONS: Information published in a foreign language considered to merit NASA distribution in English.

SPECIAL PUBLICATIONS: Information derived from or of value to NASA activities. Publications include final reports of major projects, monographs, data compilations, handbooks, sourcebooks, and special bibliographies.

TECHNOLOGY UTILIZATION PUBLICATIONS: Information on technology used by NASA that may be of particular interest in commercial and other non-aerospace applications. Publications include Tech Briefs, Technology Utilization Reports and Technology Surveys.

Details on the availability of these publications may be obtained from:

SCIENTIFIC AND TECHNICAL INFORMATION OFFICE

NATIONAL AERONAUTICS AND SPACE ADMINISTRATION

Washington, D.C. 20546